International Journal of Minerals, Metallurgy and Materials
Volume 30, Number 3, March 2023, Page 428
https://doi.org/10.1007/s12613-022-2546-9

Invited Review

Current advances of transition metal dichalcogenides in electromagnetic wave absorption: A brief review

Shijie Zhang[1,2),*], *Jiying Li*[1),*], *Xiaotian Jin*[1)], *and Guanglei Wu*[2),✉]

1) School of Material Science and Engineering, Henan Province Engineering Research Center of New Cermet Matrix Composites, Henan University of Technology, Zhengzhou 450001, China

2) Institute of Materials for Energy and Environment, State Key Laboratory of Bio-fibers and Eco-textiles, College of Materials Science and Engineering, Qingdao University, Qingdao 266071, China

(Received: 25 June 2022; revised: 2 September 2022; accepted: 5 September 2022)

Abstract: Transition metal dichalcogenides (TMDs) show great advantages in electromagnetic wave (EMW) absorption due to their unique structure and electrical properties. Tremendous research works on TMD-based EMW absorbers have been conducted in the last three years, and the comprehensive and systematical summary is still a rarity. Therefore, it is of great significance to elaborate on the interaction among the morphologies, structures, phases, components, and EMW absorption performances of TMD-based absorbers. This review is devoted to analyzing TMD-based absorbers from the following perspectives: the EMW absorption regulation strategies of TMDs and the latest progress of TMD-based hybrids as EMW absorbers. The absorption mechanisms and component-performance dependency of these achievements are also summarized. Finally, a straightforward insight into industrial revolution upgrading in this promising field is proposed.

Keywords: transition metal dichalcogenides; phase manipulation; hybrids; hierarchical structure; absorption mechanism

1. Introduction

A new round of scientific and technological revolution is emerging all over the world, and 5G has become the essential development direction of the new generation of information and communication technology. Although such technology brings great convenience to human life, electromagnetic wave (EMW) interference and pollution have increasingly become urgent problems. To tackle this issue, the exploration of functional materials for electromagnetic interference (EMI) shielding and EMW absorption is necessary [1–7]. Compared with EMI shielding materials, electromagnetic wave absorption materials (EWAMs) converting EMW projected onto their surface to thermal or other energies can reduce the secondary pollution of EMW in the environment and play an important role in the military and civil fields [8–10]. Traditional EWAMs mainly include ferrites, metal powder, barium titanate, silicon carbide, and conductive fibers [11–12]. Nevertheless, traditional EWAMs have gradually been insufficient to fulfill the demands of thin thickness, lightweightness, wide absorption bandwidth, and strong attenuation ability [13–15]. Therefore, two-dimensional (2D) nanomaterials with high specific surface areas and lightweightness have become competitive EWAMs with good application prospects [16–20].

Generally, transition metal dichalcogenides (TMDs), expressed as MX_2 (M = Mo, W, Nb and X = S, Se, Te), possess lamellar structure that are connected by covalent bonds and stacked along the *c*-axis by van der Waals force, with an interlayer spacing of only a few angstroms (Fig. 1(a)). 2D TMDs have attracted considerable attention and have been promptly developed in various fields because of their high specific surface area, excellent semiconductor behavior, and unique electric feature [21–22]. The quantum confinement effect, relative slippage between adjacent lamellae, and decrease of layers can dramatically influence the transmission behavior of carriers, allowing TMDs to present fascinating and diverse conductive properties [23–26]. Recently, TMDs have also emerged as promising EWAMs and exhibited several similarities and differences in comparison with other 2D materials. First, layered structures endow TMDs with an increased specific surface area and ample inherent defects, including vacancies, intercalated impurities, and substitutional impurities, which can effectively improve their dielectric loss. Second, various interfaces will be formed in TMDs due to their unique lamellar stacking structure, which will undoubtedly enhance EMW attenuation. Third, the difference of d orbitals in various transition metals results in versatile electronic structures and physical properties of TMDs, eventually resulting in a distinct EMW absorption ability. Meanwhile, MXenes and graphene always exhibit excessive conductivity, which is not conducive to impedance matching.

*These authors contributed equally to this work.

✉ Corresponding author: Guanglei Wu E-mail: wuguanglei@qdu.edu.cn, wuguanglei@mail.xjtu.edu.cn

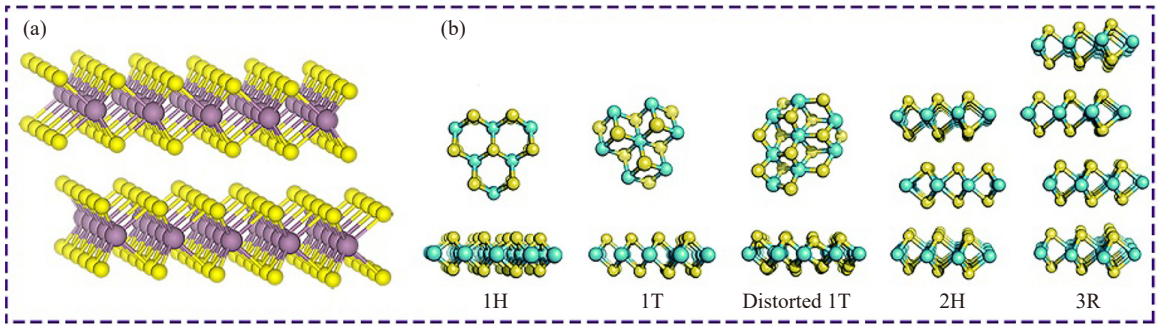

Fig. 1. (a) Typical structure of TMDs and (b) phase structures of TMDs. Republished with permission of Royal Society of Chemistry, from Phase engineering of transition metal dichalcogenides, D. Voiry, A. Mohite, and M. Chhowalla, 44, 2015, permission conveyed through Copyright Clearance Center, Inc.

Furthermore, edge states existing in nanoribbons and nanoclusters can significantly affect the chemical, electronic, and magnetic properties of TMDs. In particular, for the magnetic property, in addition to unsaturated spin states caused by unsaturated coordination atoms in the edges of TMDs, unsaturated spin states occur near vacancy defects in some TMDs materials. The existence of these unsaturated spin states will lead to the generation of magnetism, which is the major difference from other 2D absorbers.

Essentially, the modifications based on TMDs have been conducted to pursue exceptional EMW absorption performances to date. As regards single-component TMDs, phase transition and defect engineering are two main concerns in regulating physical and chemical properties. The changes in the chemical bonds and crystal textures of transition metal atoms could form various phases (Fig. 1(b)) [27], such as the semiconducting H-phase involving the monolayer (1H) and multilayer (2H), metallic 1T-phase induced by the transformation of one chalcogen plane, distorted 1T-phase, and 3R-phase [28–29]. The rational regulation of ineluctable defects can enable TMDs to modulate phase structures, adjust the band, and facilitate carrier transmission [29–30]. Apart from single-component TMDs, the construction of heterointerfaces based on multiple components and hierarchical structures is another approach to ameliorate the EMW ability of TMDs because most TMDs are dielectric with a single loss mechanism, which restricts the improvement of impedance matching [14,31–32].

Among the 2D TMD-based EWAMs, MoS_2 is the most investigated substance [12,14,32–35]. Several reviews have presented a nice wrap-up of the progress of MoS_2 in EMW absorption [16,36–39], but a comprehensive and systematical summary of 2D TMDs and their hybrids as EWAMs is still a rarity. Hence, it is imperative and significant to understand the interaction among the morphologies, structures, phases, components, and EMW absorption performances of TMD-based absorbers. In this work, we systematically summarize the EMW absorption regulation strategies of TMDs, including phase manipulation, defect engineering, chemical doping, and morphology configuration. In addition, state-of-the-art TMD-based EWAMs are reviewed, and the synergistic effect of various components is emphasized by balancing their impedance matching and attenuation ability. Finally, some future research perspectives are proposed.

2. Brief knowledge of EMW absorption mechanisms for TMD-based absorbers

Generally, absorption performance mainly depends on the impedance matching and attenuation ability of EWAMs [40–41]. First, an ideal impedance matching can direct an incident EMW inward absorbers without surface reflection, which is a prerequisite for designing EWAMs. Then, the EMW energy can be further dissipated or converted to other energies dominated by a dielectric–magnetic dual loss. In this section, the most widely recognized transmission line model is chosen as the basic theory to portray the interaction between annular absorbers and variable EMWs [42–43].

2.1. Impedance matching

After several simulations and simplifications on the transmission line model, impedance matching can be acquired by $|Z_{in}/Z_0|$, as shown in Eq. (1). Z_{in}, Z_0, f, d, and c represent the input impedance, impedance of free space, EMW frequency, thickness of the absorber, and light velocity, respectively. ε_r and μ_r are the relative complex permittivity and complex permeability, respectively, which can be expressed as $\varepsilon_r = \varepsilon' - j\varepsilon''$ and $\mu_r = \mu' - j\mu''$. On the basis of Kirchhoff's law, Z_0 can be calculated as 377 Ω. If the value of $|Z_{in}/Z_0|$ is near 1, the absorber possesses a well-matched impedance [44–46]. Analogously, another parameter evaluating the impedance matching of absorber and air is the delta function (Δ) (Eq. (2)), where the values of K and M are obtained with ε_r and μ_r (Eqs. (3) and (4)). The value of Δ approaching 0 indicates excellent impedance matching [47–49]. In these equations, the regulation of the electromagnetic parameters of absorbers is significant to the acquisition of good impedance matching. In other words, the complementary balance between the dielectric property and magnetism is instrumental in EMW absorption. For instance, Zhang *et al*. [50] designed and constructed a one-dimensional (1D) Co@NC@MoS_2 absorber to balance the dielectric constant and permeability, and impedance matching could be tailored by adjusting the lamellar MoS_2 loading. Moreover, the quarter-wavelength ($\lambda/4$) matching model can normalize the thickness of EWAMs (Eq. (5)), so two reflected EMWs with a phase difference of 180º can off-

set each other at the interface of the absorber and air, which can attenuate the EMW to the maximum [51–54]. Many studies have revealed that the minimum reflection loss (RL_{min}) is closely linked with the quarter-wavelength cancellation and impedance matching (Fig. 2(a)), and the corresponding matching frequency moves to the low region with the matched thickness (t_m) increasing [2,47,55].

$$\left|\frac{Z_{in}}{Z_0}\right| = \left|\sqrt{\frac{\mu_r}{\varepsilon_r}}\tanh\left(j\frac{2\pi fd}{c}\sqrt{\mu_r\varepsilon_r}\right)\right| \quad (1)$$

$$|\Delta| = \left|\sinh^2(Kfd) - M\right| \quad (2)$$

$$K = \frac{4\pi\sqrt{\mu'\varepsilon'}\sin\frac{\delta_e+\delta_m}{2}}{c\cos\delta_e\cos\delta_m} \quad (3)$$

$$M = \frac{4\mu' c\cos\delta_e\varepsilon'\cos\delta_m}{(\mu' c\cos\delta_e - \varepsilon'\cos\delta_m)^2 + \left[\tan\left(\frac{\delta_m}{2}-\frac{\delta_e}{2}\right)\right]^2(\mu' c\cos\delta_e - \varepsilon'\cos\delta_m)^2} \quad (4)$$

$$t_m = \frac{nc}{4f_m\sqrt{|\mu_r||\varepsilon_r|}}(n = 1,3,5,\ldots) \quad (5)$$

2.2. EMW attenuation ability

The attenuation constant (α) is of great significance in assessing the EMW dissipation ability of absorbers, as shown in Eq. (6). Generally, the higher the α value is, the more beneficial the dissipation of EMW energy is [56–58]. In addition, the RL values can directly reflect the EMW absorption capacity to a great extent (Eq. (7)), and the smaller the RL is, the better the EMW consumes. Usually, RL < −10 dB matches 90% of the EMW absorption, and the corresponding frequency range would be an effective absorption bandwidth (EAB) [59–61]. In addition, the dielectric loss tangent ($\tan\delta_\varepsilon = \varepsilon''/\varepsilon'$) and magnetic loss tangent ($\tan\delta_\mu = \mu''/\mu'$) can provide a preliminary reference for estimating the dielectric loss and magnetic loss [62–64].

$$\alpha = \frac{\sqrt{2}}{c}\pi f\times\sqrt{(\mu''\varepsilon'' - \mu'\varepsilon') + \sqrt{(\mu''\varepsilon'' - \varepsilon'\mu')^2 + (\mu'\varepsilon'' + \varepsilon'\mu'')^2}} \quad (6)$$

$$RL = 20\lg\left|\frac{Z_{in}-Z_0}{Z_{in}+Z_0}\right| \quad (7)$$

To analyze the dielectric loss in detail, ε_r can be further expressed as Eqs. (8) and (9), where σ, τ, ε_s, and ε_∞ are the electric conductivity, relaxation time, static permittivity, and permittivity at an "infinite" high frequency, respectively. In these equations, the dielectric loss mainly includes polarization relaxation and conduction loss. For TMD-based EWAMs, the unique electric properties from the semiconductor to the conductor allow them to easily induce charge transportation under an alternating electromagnetic field, leading to the generation of local current. A high σ can augment ε'' in light of free electron theory. Polarization relaxation mainly involves dipole polarization and interfacial polar-

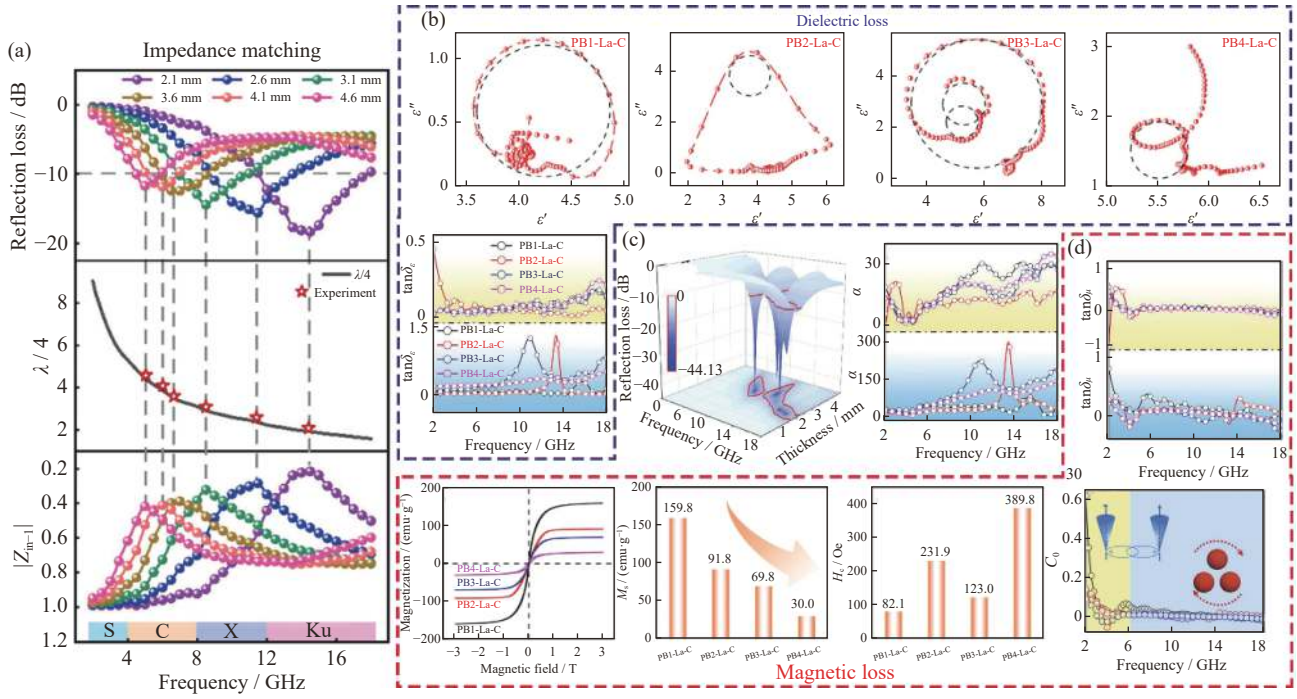

Fig. 2. Absorption mechanisms of EMW absorbers: (a) impedance matching. Reprinted with permission from L.L. Xu, J.Q. Tao, X.F. Zhang, *et al.*, *ACS Appl. Nano Mater.*, 4, 11199–11209 (2021) [55], Copyright 2021 American Chemical Society; (b) dielectric loss; (c) RL curves and attenuation constant; (d) magnetic loss. Reprinted from *J. Mater. Sci. Technol.*, 82, Z.G. Gao, Z.H. Zhao, D. Lan, K.C. Kou, J.Q. Zhang, and H.J. Wu, Accessory ligand strategies for hexacyanometallate networks deriving perovskite polycrystalline electromagnetic absorbents, 69, Copyright 2021, with permission from Elsevier.

ization under low frequencies [65–68]. In particular, electronic polarization and ion polarization belonging to polarization relaxation should be excluded because they always exist in terahertz. The vacancies, adatoms, grain boundaries, and impurities in TMDs could form abundant dipoles and polarization sites, and chargers would undergo "aggregation–dispersion," causing the dissipation of EMW energy [69–70]. Analogously, the natural advantage of lamellar structures enables TMDs to easily construct heterointerfaces or hierarchical structures. The interfacial polarization stemming from the displacement of spatial charges in heterointerfaces makes a valuable contribution to the dielectric loss of TMD-based EWAMs. Based on the Debye theory, Cole–Cole semicircles were introduced to investigate the polarization relaxation, which can be described as Eq. (10) [71–73], where ω is the angular frequency. Each semicircle in the curve of ε' vs. ε'' indicates a polarization relaxation process, and the higher the number and larger the radius of semicircles are, the stronger the multiple polarization is. Significantly, the Cole–Cole plots can also embody the conduction loss when the tail tends to a straight line, and the conduction loss is positively interrelated to the slope of the line segment [74–75].

$$\varepsilon' = \varepsilon_\infty + \frac{\varepsilon_s - \varepsilon_\infty}{\omega^2\tau^2 + 1} \tag{8}$$

$$\varepsilon'' = \frac{\varepsilon_s - \varepsilon_\infty}{\omega^2\tau^2 + 1}\omega\tau + \frac{\sigma}{\omega\varepsilon_0} \tag{9}$$

$$\left(\varepsilon' - \frac{\varepsilon_s + \varepsilon_\infty}{2}\right)^2 + (\varepsilon'')^2 = \left(\frac{\varepsilon_s - \varepsilon_\infty}{2}\right)^2 \tag{10}$$

Although most magnetic TMDs are single dielectric loss, the magnetic loss will be another cardinal attenuation mechanism for magnetic TMDs or composites of TMDs and magnetic components. The magnetic loss mainly stems from the hysteresis loss, domain-wall resonance, eddy current loss, natural resonance, and exchange resonance [76–78]. The hysteresis loss and domain-wall resonance are inappropriate in 2–18 GHz, which can be ignored. The magnetoelectric conversion can be induced to consume the EMW energy when magnetic EWAMs are in an alternating magnetic field, which is the eddy current loss. It can be evaluated by the C_0 parameter, as shown in Eq. (11). If the C_0 value is close to a constant as the frequency changes, the eddy current loss can make a major contribution to the magnetic loss. Furthermore, exchange resonance always exists at higher frequencies (10–18 GHz) than natural resonance (2–10 GHz) [79–80]. Therefore, multiple resonances and eddy current loss mainly derive the magnetic loss of magnetic TMD-based EWAMs.

$$C_0 = \frac{\mu''}{(\mu')^2 f} \tag{11}$$

To sum up, the dielectric loss and magnetic loss are the main attenuation mechanisms for EWAMs, as shown in Fig. 2(b–d) [81]. In addition, multiple scattering and reflection derived from hierarchical structures can not only prolong the propagation path of EMWs in materials boosting the EMW energy dissipation but can also ameliorate impedance matching. For example, three-dimensional (3D) MoS_2/carbon nanofiber (CNF) aerogels with multiple heterogeneous interfaces and hierarchical porous structures exhibited excellent EMW absorption performances under an ultralow filler loading [82]. Sun *et al*. [83] constructed a zero-dimensional (0D)–1D–2D Co_9S_8/CNTs/MoS_2 hybrid and realized the maximized synergistic effect of multiple reflections, conduction loss, and interfacial and dipole polarization. Nonetheless, although TMD-based EWAMs have made considerable progress, the thorough inner link between EMW absorption mechanisms and their bewitching structures should be associated.

3. Strategy for the absorption performance regulation of TMDs

In this section, we mainly focus on the strategies to tailor the microcomponent and microstructure of TMDs so as to improve their EMW absorption performances in view of the reported achievements, including phase manipulation, chemical doping, and morphology and structure configuration.

3.1. Phase manipulation

As mentioned above, the phase structures of TMDs are determined by the d orbital electron. When the d orbital is fully filled, TMDs usually exhibit semiconductor properties, whereas partially filled TMDs generally show metal properties. Different phases have various influences on EMW absorption performances. For example, the intrinsic low conductivity of stable 2H-MoS_2 is the main restriction for its further application in EMW absorption, whereas that of metastable 1T-MoS_2 is its excessively high electrical conductivity. Thus, the multiple phases can effectively tailor the electromagnetic parameters of TMDs and ameliorate their EMW attenuation capacity. Ding *et al*. [84] reported that 1T@2H WS_2 nanosheets showed more remarkable absorption properties than pure 2H WS_2 nanosheets, the RL_{min} of 1T@2H WS_2 reached −47.1 dB, and the EAB covered 5.2 GHz with 35wt% filler loading at 2.2 mm. Yan *et al*. [33] also investigated the absorption performance of mixed 1T and 2H MoS_2, which exhibited an ultrawide EAB of more than 10 GHz. Recently, increasing efforts to further investigate the effect of the phase transition of TMDs on the absorption mechanism have been made. Ning *et al*. [85] fabricated a series of 1T/2H MoS_2 with different phase ratios through a facile magneto-hydrothermal method and systematically investigated the phase-dependent EMW absorption performance (Fig. 3 (a–c)). The authors believed that introducing metal–semiconductor phase-forming abundant interfaces could facilitate the dipole distribution dynamics, and the dual phases enhanced the electron transfer ability, which eventually optimized the polarization relaxation and boosted the attenuation ability.

3.2. Defect engineering

As mentioned above, abundant and various intrinsic defects exist in the crystal structure of TMDs, such as point de-

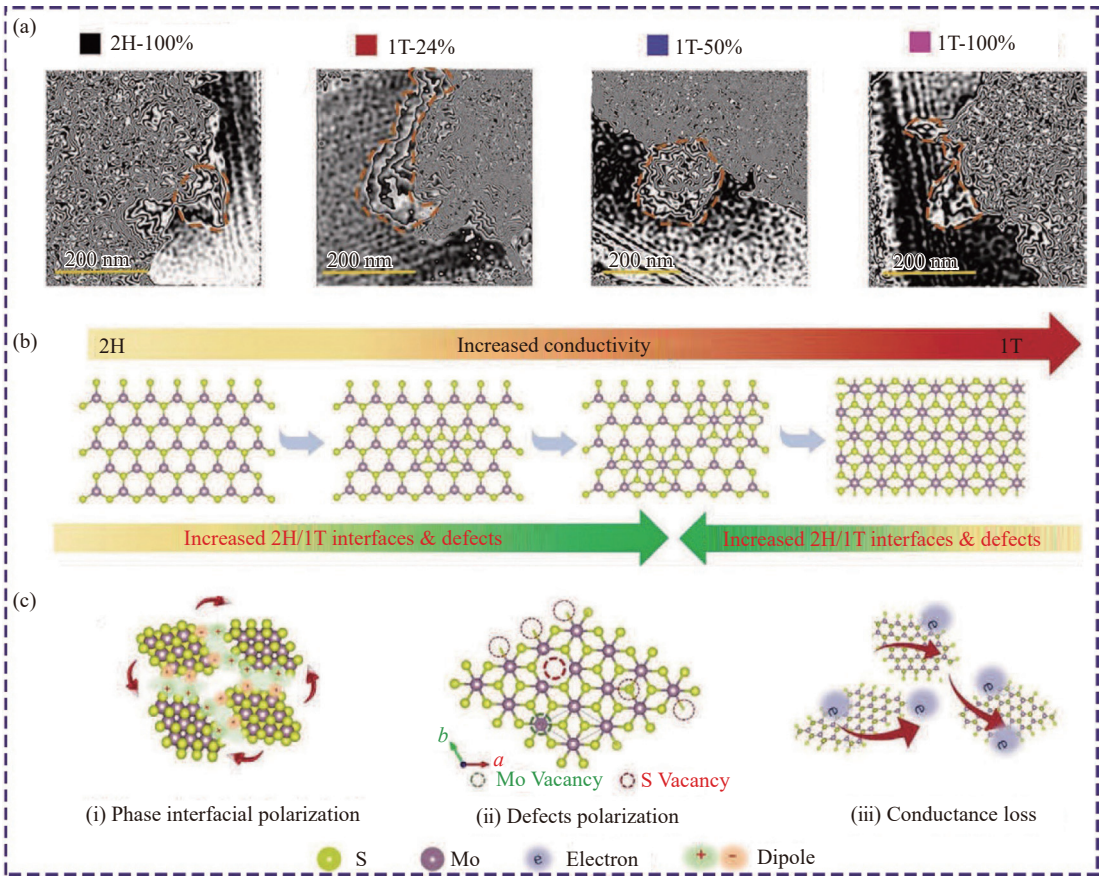

Fig. 3. (a) Off-axis electron holograms; (b) phase-dependent conductivity, phase interfaces, and defects; (c) loss mechanisms of mixed 1T/2H MoS_2. M.Q. Ning, P.H. Jiang, W. Ding, *et al.*, *Adv. Funct. Mater.*, 31, 2011229 (2021) [85]. Copyright John Wiley and Sons. Reproduced with permission.

fects (vacancies, substitution, adatoms, and substitutional impurities) and line defects (line vacancies, grain boundaries, and edge states). Tremendous research works have demonstrated that the custom design of these defects is an effective approach in tailoring the physical–chemical properties of TMDs and boosting device performances [29]. Generally, defect engineering for TMDs mainly includes the suppression and repair of defects and defect manufacturing. Taking the application in EMW absorption, we focus on defect manufacturing in this review. Cao *et al.* [86] developed NbS_2 nanosheets with abundant active sites located at their edges and substrates for EMW absorption. Wu *et al.* [14] conducted an experiment where they controlled defects in MoS_2 to regulate the EMW absorption ability. The recent investigation is largely concentrated on the dielectric loss regulation of TMDs, and the effect of defect engineering on magnetic loss has attracted our attention. For instance, the introduction of a small amount of heteroatom (e.g., Cu, Mn, and Co) should adjust the spin states of electrons in TMDs by hybridizing or coupling the 3d states of these heteroatoms with the transition metal 4d states and chalcogenide 3p states of TMDs, leading to the change in the magnetic property.

3.3. Chemical doping

Chemical doping is an important approach to regulating the EMW absorption property of TMDs. Theoretical studies and experimental research have demonstrated that doping TMDs with transition metals can endow them with magnetic properties [87]. Wang *et al.* [88] investigated the effect of magnetic moments on the EMW absorption performance of Ni-doped MoS_2. When the content of doped Ni was 3wt%, the Ni-doped MoS_2 could obtain an optimized saturation magnetization (M_s) absorption performance without changes in the crystal structure of MoS_2. They believed that the zigzag edges and variations in abundant vacancies were responsible for the magnetic properties, and the regulation of electromagnetic parameters led to good absorption performance. In addition, suitable doping may change the electron in the d orbital, which can stabilize the distorted 1T-phase structure by reducing the energy barrier between the H-phase and quasi-metallic distorted 1T-phase [28]. Thus, Wu *et al.* [14] proposed a novel strategy to develop a MoS_2 solid solution as an efficient EMW absorber through the coordination between Cu^{2+} and polydopamine (PDA) as shown in Fig. 4(a). After doping, the MoS_2 with a controllable S vacancy, Cu interstitial, and N substitutional exhibited typical metal phases, and the layer number could be effectively decreased (Fig. 4(b)). In addition, the solid solution possessed an excellent EMW absorption performance, i.e., RL_{min} of −48.22 dB and EAB of 7.12 GHz, attributed to the synergistic polarization of the point–point interaction, point–face interaction, and face–face interaction.

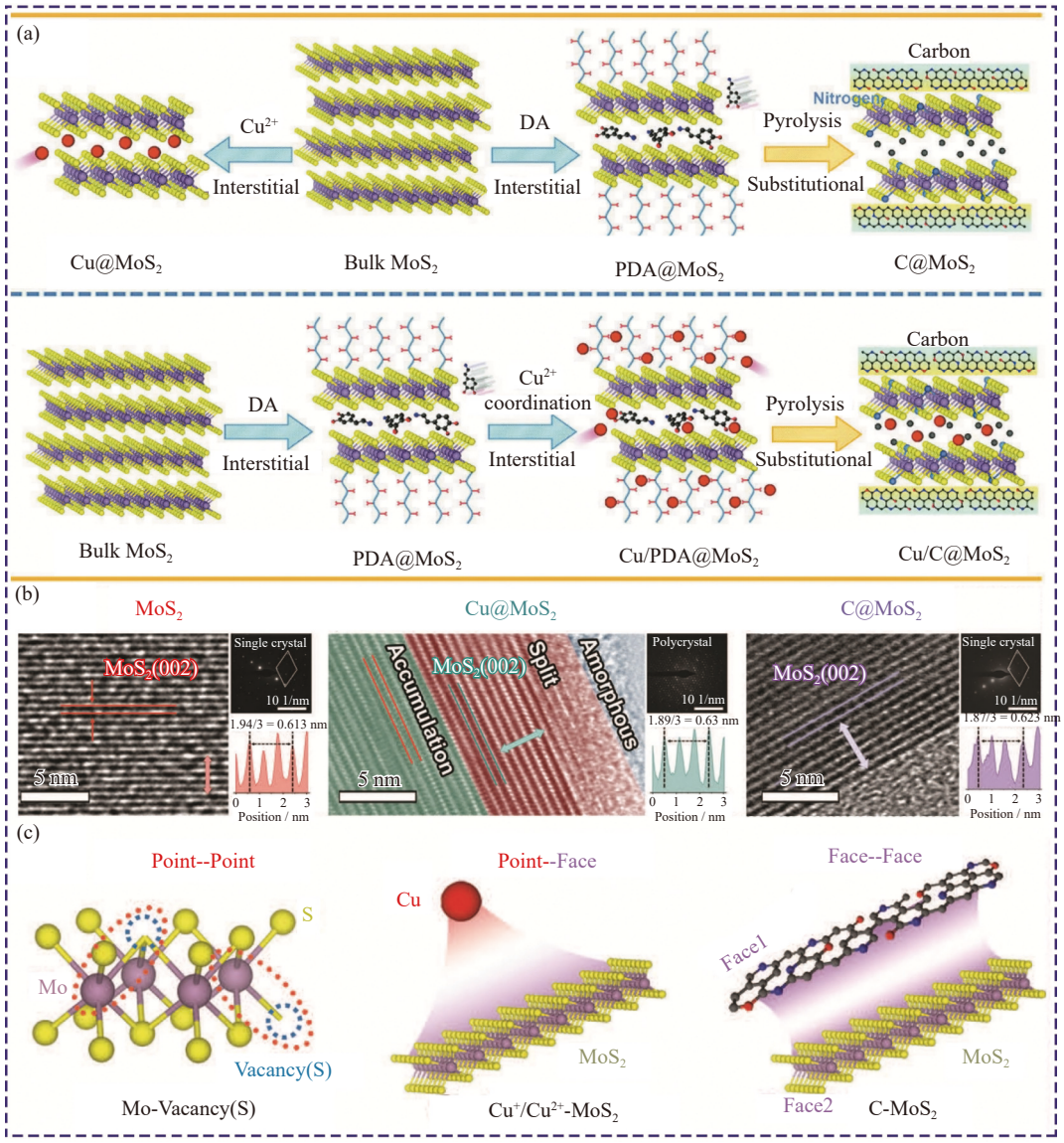

Fig. 4. (a) Fabrication of the MoS_2-based solid solution; (b) HRTEM images, SAED images, and line profiles of the samples; (c) structures of polarization centers in the corresponding samples. Reprinted from Z.G. Gao, Z.H. Ma, D. Lan, *et al.*, *Adv. Funct. Mater.*, 32, 2112294 (2022) [14]. Copyright John Wiley and Sons. Reproduced with permission.

3.4. Morphology and structure configuration

The design of a hierarchical structure and geometrical morphology is crucial to achieving exceptional absorption performances [89–90]. In terms of TMDs, 3D flower-like nano-/micro-structures assembled by randomly oriented 2D nanosheets possess large specific surface areas and always own an outstanding absorption performance, such as flower-like $MoSe_2$ [91–92], 1T/2H MoS_2 nanoflower [93], and MoS_2/FeS_2 microflower [94]. In addition, the nanoscale design of the hierarchical structure with tailored heterointerfaces has become an efficient approach to optimize electromagnetic parameters, and the construction of core–shell nanostructured TMDs is a popular method. Qi *et al.*[95–96] have made considerable contribution in this regard and explored many high-performance TMD hybrids, such as flower-like $FeSe_2@MoSe_2$ nanocomposites and $MSe_2/FeSe_2@MoSe_2$ (M = Co, Ni) nanocomposites. Recently, they proposed a strategy to optimize EMW absorption by constructing inner and outer interchangeable heterojunctions based on 2D–2D $MoSe_2/MoS_2$ nanocomposites [97]. The results showed that a well-designed heterojunction and flower-like morphology generated enhanced interfacial polarization and multiple reflections/scattering, thus, leading to an exceptional EMW absorption. Similar to the core–shell structure, hollow-structured TMDs also possess promoted dielectric loss and multiple reflections [98]. Cao *et al.* [86] successfully fabricated the hollow-sphere structure based on NbS_2 nanosheets. They found that the reaction time and the ratio of Nb and S sources could affect the morphology and content ratio of 1T to 2H phases (Fig. 5(a–b)) and endowed NbS_2 hollow nanospheres with abundant electrochemical active sites and high conductivity, which facilitated the polarization relaxation, electron transfer and hopping, multiple reflections, and good impedance matching. Attributed to these merits, the hollow NbS_2 eventually achieved an unpreceden-

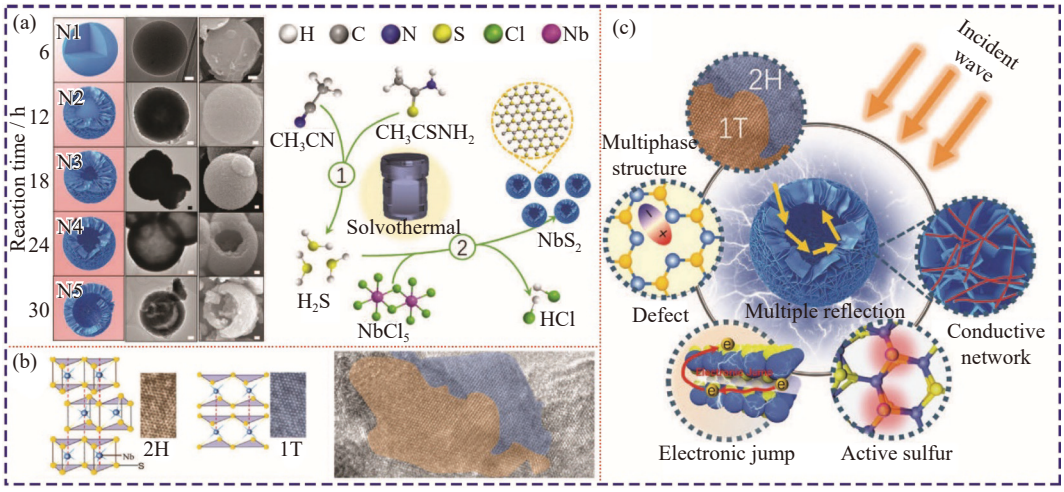

Fig. 5. (a) Schematic illustration of the growth mechanism of a hollow-sphere NbS_2; (b) crystal structure and HRTEM of the 1T and 2H phases in NbS_2; (c) schematic illustration of the EMW absorption mechanisms of a hollow-sphere NbS_2. Reprinted from H.B. Zhang, J.Y. Cheng, H.H. Wang, *et al.*, *Adv. Funct. Mater.*, 32, 2108194 (2022) [86]. Copyright John Wiley and Sons. Reproduced with permission.

ted EMW absorption performance (RL_{min} of −43.85 dB and EAB of 6.48 GHz), as shown in Fig. 5(c).

By and large, the strategies mentioned above can tackle the problem of having a narrow EAB and poor reflection loss of TMDs to some extent. However, most modified TMDs acquired better absorption at large thickness or filler loading, which was not conducive to the development of "thin, light, wide, and strong" absorbers.

4. State of the art of TMD-based hybrids as EWAMs

In addition to the modification of TMDs, the conventional method of improving EMW absorption is the combination of TMDs with other functional materials. In this regard, the state-of-the-art achievements were divided into two categories: one is the coupling of TMDs with high-conductivity materials to eliminate the skin effect, and the other is the coupling of TMDs with magnetic loss materials to obtain a synergetic EMW absorption. Of course, there are several advanced composites of TMDs with other semiconductors, such as TiO_2/WS_2 [99], $MoS_2/Nd_2O_2CO_3$ [100], and ZnO/MoS_2 [101]. However, the research in this aspect has been far from adequate.

4.1. Coupling with high-conductivity components

4.1.1. TMDs/carbon

Carbon materials are attractive materials owing to their many advantages, such as low density, low cost, and good stability [102]. Generally, carbon-based EWAMs possess a high attenuation ability, but their exorbitant conductivity leads to weak impedance matching. The hybrids of semiconductor TMDs/carbon materials can significantly ameliorate the comprehensive conductivity and increase heterointerfaces, thus, boosting the EMW absorption [103–105]. In addition, TMDs/carbon composites can effectively ameliorate the high density of pure TMDs. Many strategies to construct TMDs/carbon composites have been developed in recent years. Zhang *et al.* [106] designed carbon fiber (CF)@MoS_2 composites with an ultrawide EAB of approximately 10.85 GHz at 3.8 mm. Liu *et al.* [107] fabricated 3D carbon foam@1T-2H MoS_2 nanosheets, which showed an excellent absorption performance (RL_{min} of −45.88 dB and EAB of 5.68 GHz at 2.2 mm). Xu *et al.* [55] constructed hollow carbon@MoS_2 nanospheres, and the composites obtained a high-performance EMW absorption by controlling the graphitization of carbon cores and the thickness of the MoS_2 shell. Lu *et al.* [108] acquired lotus leaf-derived gradient hierarchical porous C/MoS_2 hybrids with RL_{min} of −50.1 dB at 2.4 mm and EAB of 6 GHz at 2.2 mm, attributed to the synergistic effect of improved conductive loss, enhanced polarization loss, and well-matched impedance. Xu *et al.* [109] reported a P-doped bacterial cellulose-derived carbon nanofiber/$MoSe_2$ nanocomposite with a superior minimum reflection loss. Significantly, Zhang *et al.* [35] constructed a 3D layered structure, nitrogen-doped carbon (NC)@MoS_2, where MnO_2 nanowires were used as a hard template (Fig. 6(a1)). Benefiting from ell-designed structures and rational compositions (Fig. 6(a2)), the hollow tubular hybrids possessed an outstanding EMW absorption.

Carbon nanotubes (CNTs) and graphene, as two main members of the nanocarbon family, have attracted tremendous attention in the construction of hierarchical structures based on TMDs [110]. Thus far, Cao *et al.* have performed significant efforts to develop CNT/TMD composites with extraordinary absorption performances, such as WSe_2@CNTs and WS_2/CNTs [111–113]. Essentially, the CNTs@MoS_2 fabricated by Qi *et al.* [114] achieved an excellent absorption property, i.e., RL_{min} of −54.75 dB at 1.49 mm and EAB of 4 GHz at 1.26 mm. For reduced graphene oxide (rGO), remarkable work was conducted by Chen *et al.* [115]. In this work, they adopted density functional theory (DFT) calculations to design and construct vertically aligned MoS_2 monolayers on N-doped rGO, which showed the highest electric

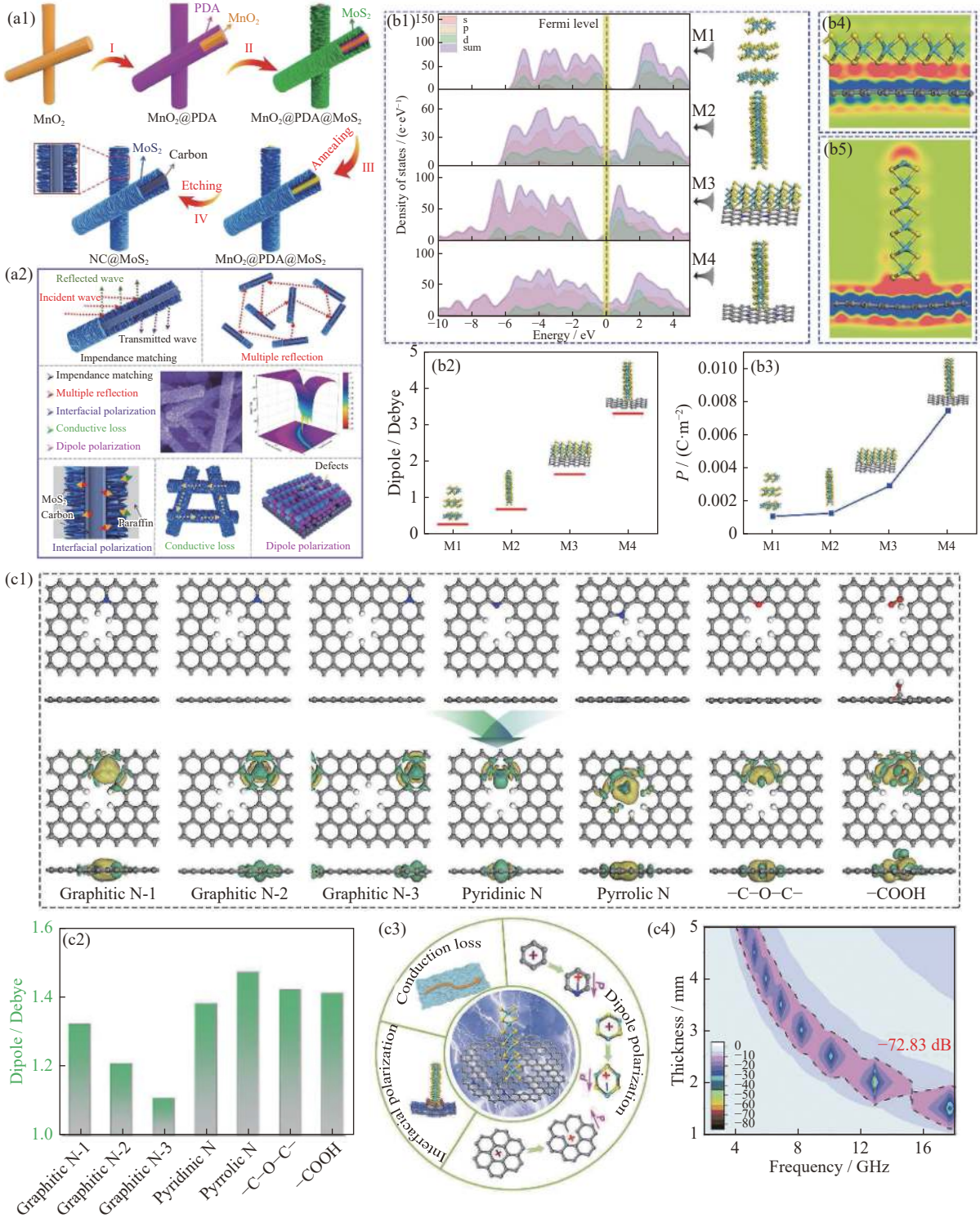

Fig. 6. (a1) Schematic illustration of the fabrication process of NC@MoS_2 nanotubes; (a2) EMW absorption mechanism of NC@MoS_2. Reprinted from *Chem. Eng. J.*, 426, K. Yang, Y.H. Cui, Z.H. Liu, P. Liu, Q.Y. Zhang, and B.L. Zhang, Design of core–shell structure NC@MoS_2 hierarchical nanotubes as high-performance electromagnetic wave absorber, 131308, Copyright 2021, with permission from Elsevier; (b1) density of states plots of four models; (b2) theoretical calculations of dipole moments; (b3) theoretical calculations of the electric polarizability of four models and 2D schematic illustrations of the charge density difference for M3 (b4) and M4 (b5), respectively; (c1) top and side views of the charge density difference for graphitic N-1, graphitic N-2, graphitic N-3, pyridinic N, pyrrolic N, –C–O–C–, and –COOH; (c2) theoretical calculations of the dipole moments of N dopants and oxygen-containing groups; (c3) schematic illustration of the electromagnetic wave absorption mechanism for the sample; (c4) RL values of the absorber. Reprinted from *Chem. Eng. J.*, 425, J. Xu, L.N. Liu, X.C. Zhang, *et al.*, Tailoring electronic properties and polarization relaxation behavior of MoS_2 monolayers for electromagnetic energy dissipation and wireless pressure micro-sensor, 131700, Copyright 2021, with permission from Elsevier.

conductivity and largest dipole moment among different models (Fig. 6(b1–b5)). Accordingly, this composite exhibited an outstanding EMW absorption (RL_{min} of −72.83 dB and EAB of 4.81 GHz at 1.8 mm) due to the enhanced polarization loss (Fig. 6(c1–c4)).

4.1.2. TMDs/conductive polymers

Conductive polymers (CPs) with adjustable electric conductivity and good environmental stability are promising candidate EWAMs, especially for polyaniline (PANI), polypyrrole (PPy), and polythiophene (PTh) [116–117]. Similar to carbon composites, these polymers can provide an excellent conduction loss for EMW attenuation. Moreover, the varied conductivity from insulator to conductor is instrumental for tuning impedance matching because high conductivity contributes to the strong attenuation ability and low conductivity leads to well-matched impedance. Considering the facile fabrication of CPs and the merits of TMDs, the combination of TMDs and CPs in optimizing the EMW absorption ability has been studied for a long time, and recent research has been focused on the design of hierarchical nanocomposites [118–119]. Gai *et al*. [120] designed and fabricated core-shell PPy@MoS_2 nanotubes, which exhibited a wider EAB than pure MoS_2 nanoflowers and pristine hollow PPy nanotubes. The hierarchical structure provided a mass of heterojunctions and a well-designed conductive network, causing enhanced interfacial polarization, multiple reflections, and conduction loss.

4.1.3. TMDs/MXenes

MXenes, with a typical 2D microstructure and physicochemical performance, exhibit great potential in EMW absorption and shielding due to their excellent conductivity, rich element composition, multilayer structure, and rich functional groups [121–123]. The hierarchical structure and rich composition endow MXenes with strong multiple reflections, polarization, and anisotropy, which can help in EMW attenuation [123–124]. While the exceptional conductivity may lead to impedance mismatching, the combination of MXenes and 2D TMDs is ingenious in developing their advantages. On the one hand, 2D TMDs can easily enter the interlayer and expand their layer spacing to tailor their electrical properties and prevent 2D TMD agglomeration. On the other hand, the introduction of 2D TMDs can tailor the overall electric conductivity and optimize impedance matching. Recently, TMDs/MXenes have achieved huge EMW absorption performances, such as MoS_2@$Ti_3C_2T_x$ [125], folded $Ti_3C_2T_x$/MoS_2 [126], $Ti_3C_2T_x$@MoS_2 [127], and $Ti_3C_2T_x$/WS_2 [128]. MXenes are usually used to construct promising microstructures, such as foam and aerogel, which possess a high porosity that facilitates the entry and transmission of EMWs inside samples. Li *et al*. [34] utilized different surface tensions of $Ti_3C_2T_x$ and ammonium tetrathiomolybdate to induce the self-rolling of $Ti_3C_2T_x$, thereby constructing a $Ti_3C_2T_x$/MoS_2 self-rolling rod-based foam (Fig. 7(a1)). The unique structure not only remarkably improved the polarization loss but also reduced the conductivity to obtain well-matched impedance (Fig. 7(a2)). As a result, the RL_{min} of this foam could reach −52.1 dB, and the EAB could cover the whole X band (8.2–12.4 GHz) with a density of only 0.009 $g·cm^{-3}$ (Fig. 7(a3–a4)). In addition, Yang *et al*. [129] designed a 3D porous MoS_2/$Ti_3C_2T_x$ hybrid aerogel through atomic layer deposition (ALD) based on a $Ti_3C_2T_x$ aerogel, and they investigated the interaction between the EMW absorption performance and ALD cycles during MoS_2 fabrication (Fig. 7(b1)). After optimization, the hybrid aerogel acquired under 300 ALD cycles exhibited RL_{min} of −61.65 dB at 4.53 mm and EAB of 5.9 GHz at 2 mm. The rational construction of this aerogel optimized the impedance matching by tailoring the conductivity and provided a tremendous interfacial polarization and dipole polarization, as shown in Fig. 7(b2).

4.2. Hybridization with magnetic loss materials

Magnetic components (e.g., ferrites, metals, alloys, and metal oxides) have high permeability and exhibit a strong EMW attenuation ability. However, the limited dielectric loss, high density, and narrow absorption bandwidth make them hard to be ideal modern absorbers. The combination of dielectric functional components with magnetic constituents is an effective approach to achieving efficient EWAMs by fully realizing the synergetic effect of dielectric–magnetic loss. Of course, dual-loss composites based on TMDs are more attractive. Recent years, many composites of TMDs and magnetic materials with excellent EMW absorption performances have been developed, such as plate-like MoS_2/Co_3O_4 [130], WS_2/NiO [131], $CoFe_2O_4$@MoS_2 [132], Fe_3O_4@1T/2H-MoS_2 [133], MoS_2/Fe_3O_4 [134], and MoS_2/CoNi [135]. In addition, novel magnetic components have been introduced into this system. Wang *et al*. [136] fabricated M-type hexagonal $BaFe_{12}O_{19}$@MoS_2 composites, which had an RL_{min} of −61.0 dB and EAB of 4.4 GHz at 1.7 mm. Recently, our group introduced magnetic ferrite $CuFe_2O_4$ to construct an efficient absorber of MoS_2/$CuFe_2O_4$ composites, where $CuFe_2O_4$ nanoparticles were decorated on the flower-like MoS_2 [12]. Stemming from the balanced impedance matching and strong attenuation capacity, this composite exhibited an impressive wide EAB of 8.16 GHz at just 2.3 mm. In addition, Wang *et al*. [137] reported core–shell $ZnFe_2O_4$@MoS_2 hybrids with RL_{min} of −61.8 dB at 3 mm and EAB of 2 GHz at 2 mm. As mentioned above, structural design can improve the electromagnetic parameters of absorbers partly, and it is no exception for TMDs/magnetic components. Wang *et al*. [138] embedded $CoFe_2O_4$ nanospheres in nest-like 1T/2H-MoS_2, where 1T/2H-MoS_2 showed ferromagnetism superimposed onto a large diamagnetism. The EMW absorption performances could be tailored by adjusting the content of 1T/2H MoS_2, and the tunable permittivity and optimized impedance matching of the composites led to an outstanding absorption ability. Another recent achievement was to design and prepare binary flower-like composites of WS_2 nanoclusters on Co nanosheet composites (Fig. 8(a–b)) [139]. The hierarchical structure could introduce effective heterointerfaces that enhanced the multiple reflection and polarization relaxation. The lamellate Co also

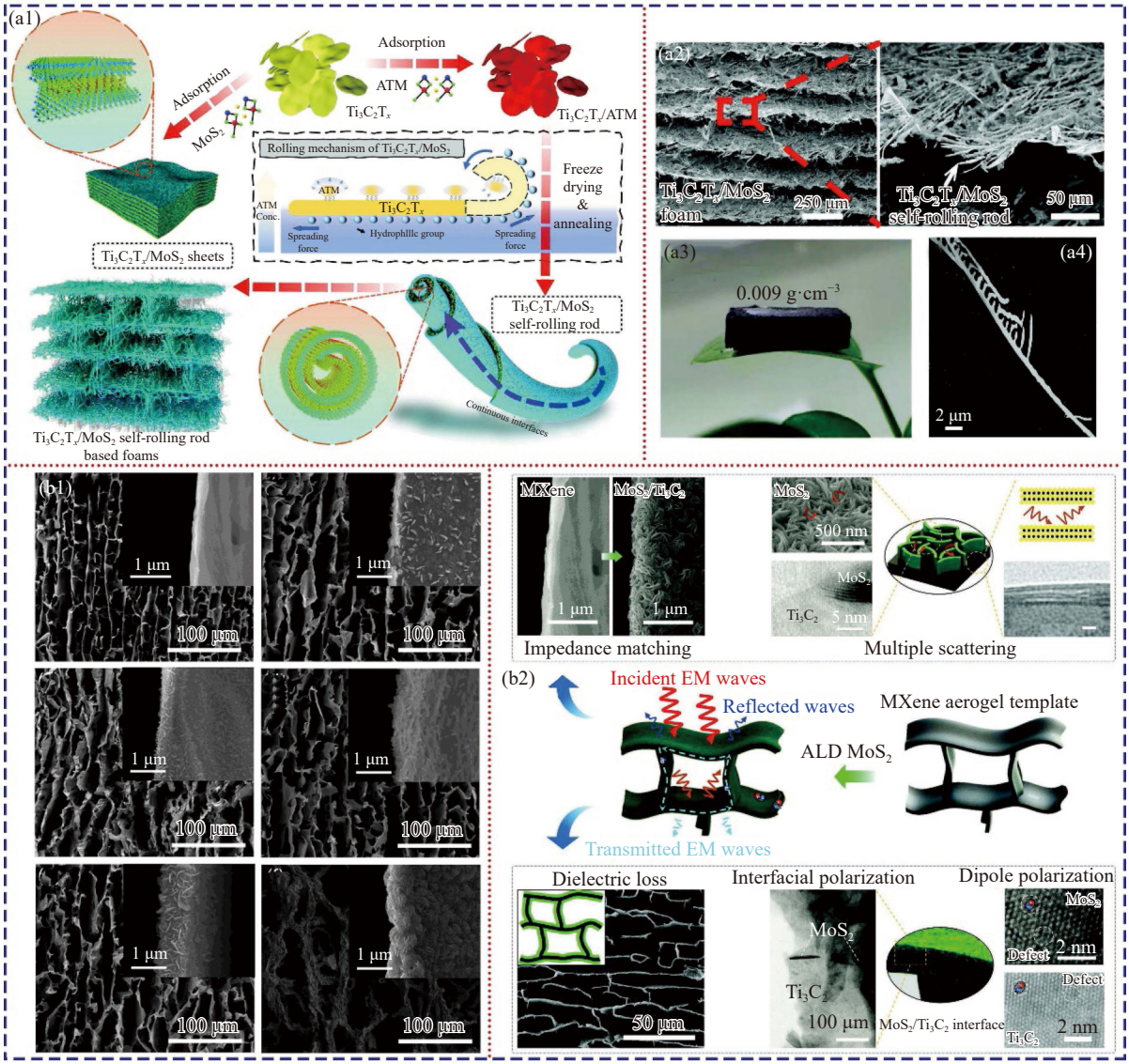

Fig. 7. (a1) Fabrication schematic diagram of $Ti_3C_2T_x/MoS_2$ sheets and self-rolling rods and rolling mechanism of $Ti_3C_2T_x/MoS_2$ self-rolling rods; (a2) cross-sectional SEM and (a3) optical photos of $Ti_3C_2T_x/MoS_2$ foam; (a4) single $Ti_3C_2T_x/MoS_2$ self-rolling rod. M.H. Li, W.J. Zhu, X. Li, *et al.*, *Adv. Sci.*, 9, 2201118 (2022) [34]. Copyright John Wiley and Sons. Reproduced with permission. (b1) SEM images of the transverse section for the samples; (b2) schematic illustration of the EMW absorption mechanisms for the $MoS_2/Ti_3C_2T_x$ aerogel. J. Yang, J. Wang, H. Li, *et al.*, *Adv. Sci.*, 9, 2101988 (2022) [129]. Copyright John Wiley and Sons. Reproduced with permission.

balanced the impedance matching and supplied the magnetic loss and conduction loss. These factors eventually endowed hybrids with excellent absorption performances (RL_{min} of −46.5 dB at 1.7 mm and EAB from 2.7 to 18 GHz with optimized thickness from 1.0 to 5.0 mm) (Fig. 8(c)).

4.3. Enhanced synergistic effect of multiple components

TMD composite-based binary components have exhibited better absorption performances than single-component TMDs owing to the synergistic or complementary effect. Accordingly, we assume that multiple components (e.g., ternary and quaternary) can achieve more remarkable properties through rational design. Therefore, we review TMD hybrids with multiple components for EMW absorption and focus on ternary composites in this section because quaternary or more complex composites generally need a complicated fabrication process and have not undergone great breakthroughs [140–143]. The hybrids of semiconductor (TMDs)–conductive component–magnetic material (SCM) are the main subject of research in developing high-performance TMD-based EWAMs, and the synergistic effects between the three phases can be enhanced, including the magnetic–dielectric loss and conduction loss [144]. Chen *et al.* [145–146] synthesized MoS_2@PPy@Fe_3O_4 and MoS_2@PPy@$CoFe_2O_4$ composites with good EMW absorption performances. By introducing the novel magnetic component $LiFe_5O_8$, hierarchical coral-like PPy/$LiFe_5O_8$/MoS_2 nanocomposites were designed and fabricated by Li *et al.* [147]. Benefiting from the conduction loss and magnetic loss, these nanocomposites possessed extremely attractive absorption performances, as shown in

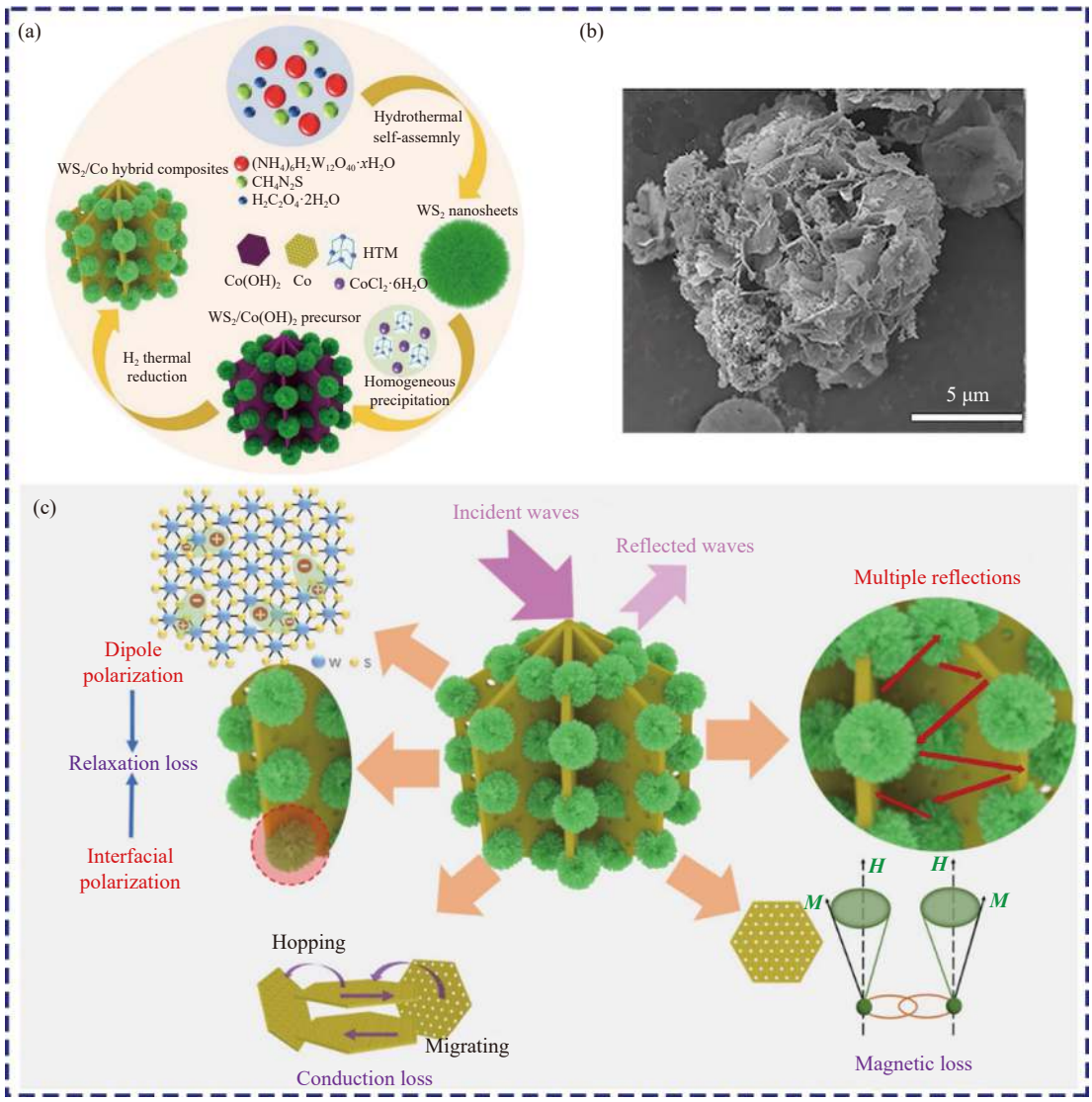

Fig. 8. Fabrication schematic diagram (a), SEM image (b), and EMW absorption mechanism (c) of WS_2 nanoclusters/Co nanosheets. Reprinted from *J. Alloys Compd.*, 912, C.L. Li, M.X. Piao, H. Zhang, and X. Wang, Constructing of Co nanosheets decorating with WS_2 nanoclusters for enhanced electromagnetic wave absorption, 165269, Copyright 2022, with permission from Elsevier.

Table 1. Yu *et al*. [151] prepared ZnCo@C@1T/2H-MoS_2 through the metal–organic frameworks (MOFs) self-template approach. This composite exhibited excellent photothermal performance and excellent EMW absorption, which make it an eligible EMW absorption candidate in cold conditions. Microstructure construction is an interesting engineering topic for ameliorating impedance matching and attenuation ability [148]. Zhang *et al*. [50] designed a novel 1D Co@NC@MoS_2 nanotube with cobalt–nitrilotriacetic acid chelate nanowires as template. Owing to the rational structure construction and a good balance of the magnetic loss and dielectric loss, the RL_{min} of this nanotube could reach −61.97 dB, and the EAB could cover 5.6 GHz at 2 mm. Recently, Ning *et al*. [149] fabricated dumbbell-like Fe_3O_4@N-doped C@2H/1T-MoS_2 yolk-shell nanocomposites through a facile etching and wet chemical synthesis strategy (Fig. 9(a–b)). The authors achieved a well-matched impedance by regulating the Fe_3O_4 component, and the composite possessed the optimized synergistic effect of the dielectric loss and magnetic loss toward an excellent EMW absorption (Fig. 9 (c)). Apart from the SCM system mentioned above, other composites have also attracted considerable attention as efficient EWAMs due to the amplified synergistic effect, such as PPy@MoS_2/C and MoS_2/MXenes/semiconductors [32,150, 152], which are typical representatives of a conductive–semiconductive–conductive network and conductive–semiconductive–dielectric network, respectively.

Although the performances of multiple-component TMD-based absorbers could exhibit excellent performances, there is still plenty of room to improve. In general, multiple components can achieve hierarchical structures based on constituents. Moreover, the electromagnetic parameters of TMDs can be easily regulated to obtain as-expected performances by replenishing specific functional materials. In addition, multiple-component absorbers can integrate their merits and endow them with overall improved performances. These factors make multiple-component TMD-based materials highly competitive absorbers.

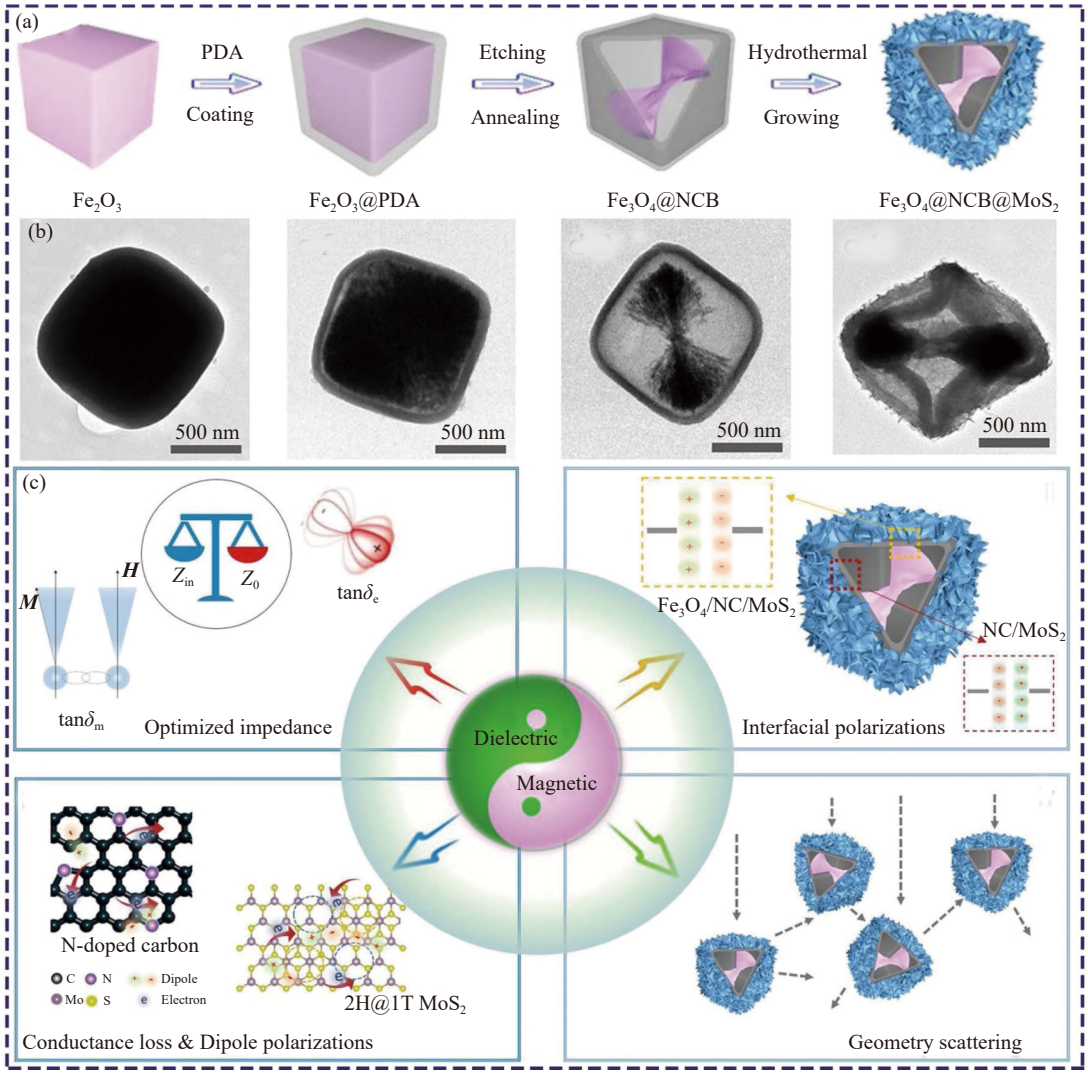

Fig. 9. Fabrication schematic illustration (a), TEM images (b), EMW absorption mechanism (c) of dumbbell-like Fe_3O_4@NC@MoS_2. Reprinted with permission from M.Q. Ning, Z.K. Lei, G.G. Tan, Q.K. Man, J.B. Li, and R.W. Li, *ACS Appl. Mater. Interfaces*, 13, 47061–47071 (2021) [149]. Copyright 2021 American Chemical Society.

Table 1. Representative TMDs and corresponding composites with EMW absorption performances

Materials	Dominated mechanism	Matrix	Absorbers ratio / wt%	RL_{min}	EAB	Ref.
1T/2H WS_2	Dielectric	Paraffin	35	−47.1 dB, 2.2 mm	5.2 GHz, 2.2 mm	[84]
1T/2H MoS_2	Dielectric	Paraffin	15	−43 dB, 2.6 mm	10.5 GHz, 2.6 mm	[33]
Ni-doped MoS_2	Dual	Paraffin	50	−58.08 dB, 2.05 mm	5.19 GHz, 2.05 mm	[88]
Co@NC@MoS_2	Dual	Paraffin	15	−61.97 dB, 2.9 mm	5.6 GHz, 1.9 mm	[50]
Cu/C@MoS_2	Dielectric	Paraffin	30	−48.22 dB, 2.5 mm	7.12 GHz, 3.1 mm	[14]
MoS_2/CNF	Dielectric	Paraffin	5	−36.19 dB, 2 mm	5.68 GHz, 2 mm	[81]
Co_9S_8/CNTs/MoS_2	Dielectric	Paraffin	9	−35.4 dB, 4 mm	8.4 GHz, 3.8 mm	[82]
Flower-like $MoSe_2$	Dielectric	Paraffin	50	−57.2 dB, 2.7 mm	4 GHz, 2.77 mm	[92]
1T/2H MoS_2 nanoflower	Dielectric	Paraffin	60	−63.78 dB, 2.57 mm	5.34 GHz, 2.04 mm	[93]
MoS_2/FeS_2 microflower	Dielectric	Paraffin	50	−60.2 dB, 2 mm	6.48 GHz, 2 mm	[94]
$CoSe_2$/$FeSe_2$@$MoSe_2$	Dielectric	Paraffin	50	−62.08 dB, 1.97 mm	4.6 GHz, 1.72 mm	[95]
$NiSe_2$/$FeSe_2$@$MoSe_2$	Dielectric	Paraffin	50	−50.82 dB, 2.01 mm	4.6 GHz, 1.77 mm	[95]
$FeSe_2$@$MoSe_2$	Dielectric	Paraffin	30	−59.84 dB, 3.1 mm	10 GHz, 3.66 mm	[96]
$MoSe_2$@MoS_2	Dielectric	Paraffin	60	−53.42 dB, 1.99 mm	7.6 GHz, 1.98 mm	[97]
MoS_2@$MoSe_2$	Dielectric	Paraffin	60	−61.71 dB, 1.88 mm	6.0 GHz, 2.16 mm	[97]
NbS_2 hollow sphere	Dielectric	Paraffin	40	−43.85 dB, 2 mm	6.48 GHz, 2 mm	[86]
CF@MoS_2	Dielectric	Paraffin	20	−21.4 dB, 3.8 mm	10.85 GHz, 3.8 mm	[106]

Table 1 (Continued)

Materials	Dominated mechanism	Matrix	Absorbers ratio / wt%	RL_{min}	EAB	Ref.
C foam/1T-2H MoS_2	Dielectric	Paraffin	40	−45.88 dB, 2.2 mm	5.62 GHz, 2.2 mm	[107]
Hollow C@MoS_2	Dielectric	Paraffin	50	−54.24 dB, 2.1 mm	5.95 GHz, 2.1 mm	[55]
Porous C/MoS_2	Dielectric	Paraffin	40	−50.1 dB, 2.4 mm	6 GHz, 2.2 mm	[108]
NC@ MoS_2	Dielectric	Paraffin	25	−52.56 dB, 2.4 mm	6.2 GHz, 2.3 mm	[35]
WS_2-NS/CNTs	Dielectric	Paraffin	40	−51.6 dB, 1.95 mm	5.4 GHz, 1.95 mm	[111]
WSe_2-MWCNTs	Dielectric	Paraffin	50	−51.9 dB, 1.79 mm	3.84 GHz, 1.79 mm	[112]
CNTs@MoS_2	Dielectric	Paraffin	40	−54.75 dB, 1.49 mm	4 GHz, 1.26 mm	[114]
WS_2-rGO	Dielectric	Paraffin	40	−41.5 dB, 2.7 mm	3.5 GHz, 1.7 mm	[110]
Monolayer MoS_2/rGO	Dielectric	Paraffin	30	−72.83 dB, 2 mm	4.81 GHz, 2 mm	[115]
MoS_2-PANI	Dielectric	Paraffin	50	−56.52 dB, 2.34 mm	5.28 GHz, 2.34 mm	[118]
PPy@MoS_2 nanotube	Dielectric	Paraffin	40	−49.1 dB, 2.5 mm	6.4 GHz, 2.5 mm	[120]
MoS_2@$Ti_3C_2T_x$	Dielectric	Paraffin	30	−51 dB, 4 mm	4.8 GHz, 4 mm	[125]
Folded $Ti_3C_2T_x$/MoS_2	Dielectric	Paraffin	30	−51.2 dB, 2.5 mm	4.6 GHz, 1.6 mm	[126]
$Ti_3C_2T_x$@MoS_2	Dielectric	Paraffin	—	−46.72 dB, 2 mm	4.32 GHz, 2 mm	[127]
$Ti_3C_2T_x$/WS_2	Dielectric	Paraffin	50	−61.06 dB, 2.14 mm	6.5 GHz, 2.5 mm	[128]
MoS_2/Co_3O_4	Dual	Paraffin	20	−43.56 dB, 4 mm	4.76 GHz, 2 mm	[130]
MoS_2/Fe_3O_4	Dual	Paraffin	90	−87.24 dB, 7.84 mm	5.52 GHz, 7.84 mm	[134]
$BaFe_{12}O_{19}$@MoS_2	Dual	Paraffin	30	−61 dB, 1.7 mm	4.4 GHz, 1.7 mm	[136]
MoS_2/$CuFe_2O_4$	Dual	Paraffin	30	−40.33 dB, 2.3 mm	8.16 GHz, 2.3 mm	[12]
$ZnFe_2O_4$@MoS_2	Dual	Paraffin	20	−61.8 dB, 3 mm	6 GHz, 2 mm	[137]
$CoFe_2O_4$@MoS_2	Dual	Paraffin	30	−68.5 dB, 1.81 mm	4.56 GHz, 1.6 mm	[138]
MoS_2/Fe_3O_4/graphite	Dual	Paraffin	30	−46.67 dB, 3.3 mm	4.56 GHz, 2.1 mm	[144]
MoS_2@PPy@Fe_3O_4	Dual	Paraffin	30	−32 dB, 2 mm	4.3 GHz, 2 mm	[145]
PPy/$LiFe_5O_8$/MoS_2	Dual	Paraffin	40	−73.25 dB, 3.07 mm	7.2 GHz, 3.14 mm	[147]
Hollow MoS_2@Fe_3O_4-graphite	Dual	Paraffin	55	−48.1 dB, 2.6 mm	4.08 GHz, 1.7 mm	[148]
Co@NC@MoS_2 nanotube	Dual	Paraffin	15	−61.97 dB, 2 mm	5.6 GHz, 2 mm	[50]
Dumbbell-like Fe_3O_4@NC@MoS_2	Dual	Paraffin	15	−68.9 dB, 4.1 mm	5.25 GHz, 2 mm	[149]
MoS_2/TiO_2/$Ti_3C_2T_x$	Dielectric	Paraffin	15	−33.5 dB, 1 mm	3.1 GHz, 1 mm	[150]
NiS/MoS_2/$Ti_3C_2T_x$	Dielectric	Paraffin	15	−58.48 dB, 2.4 mm	5.04 GHz, 2.1 mm	[32]
NiS/Ni_3S_4@PPy@MoS_2	Dual	Paraffin	50	−51.29 dB, 2.29 mm	3.24 GHz, 2.29 mm	[143]
CoZn/C@MoS_2@PPy	Dual	Paraffin	30	−49.15 dB, 1.5 mm	4.56 GHz, 1.5 mm	[140]
MoS_2/$MgFe_2O_4$/MgO/C	Dual	Paraffin	40	−56.94 dB, 2.7 mm	3.9 GHz, 2.7 mm	[141]
$ZnFe_2O_4$@C@MoS_2/FeS_2	Dual	Paraffin	50	−52.5 dB, 2.23 mm	4.98 GHz, 2.23 mm	[142]

Notes: — represents the values are not available; Dual means the magnetic loss and dielectric loss.

5. Summary and perspectives

TMDs have been regarded as a class of prospective EWAMs due to their large specific surface area, excellent semiconductor behavior, and unique electric feature. This work systematically reviews the absorption mechanisms and EMW performance regulation strategies of TMDs and the latest research advances in TMD-based EWAMs. For TMDs, phase manipulation, defect engineering, chemical doping, and hierarchical structure configuration are the most important approaches in adjusting their electromagnetic parameters and pursuing excellent absorption performances owing to their charming characteristics. For TMD-based composites, the introduction of other loss mechanisms is highly valuable to ameliorate impedance matching and enhance the attenuation ability of TMDs. Despite the huge achievements, several issues still need to be addressed to achieve excellent EMW absorption performance, clear EMW absorption mechanisms, and high practical application abilities. First, more novel TMDs should be explored, including but not limited to the introduction of different transition metals and compounding with other functional materials. Second, the phase transition and defect engineering of TMDs can tune their absorption ability. Hence, it is necessary to focus on fabrication strategies and stabilize metallic phases. Third, novel absorption mechanisms and physical models of TMDs based on their characteristic structures and composition should be developed. In addition, taking the transformation from laboratories to practical applications into consideration, smart multifunctional devices based on TMDs should be taken into consideration to adapt to extreme environments, such as corrosion resistance, flexibility, bacteriostasis, and high/low temperature resistance. Finally, the facile preparation strategies of TMD-based absorbers with high yields and green environmental protec-

tion should be developed, and EMW performances in low frequency should be focused on because most civil wireless electronic devices and important military devices work in low frequency.

Acknowledgements

This work was financially supported by the Doctoral Foundation of Henan University of Technology (No. 2021BS030), Natural Science Foundation of Shandong Province (No. ZR2019YQ24), Taishan Scholars and Young Experts Program of Shandong Province (No. tsqn202103057), and the Qingchuang Talents Induction Program of Shandong Higher Education Institution (Research and Innovation Team of Structural-Functional Polymer Composites).

Conflict of Interest

The authors declare no conflict of interest.

References

[1] Y.L. Zhang and J.W. Gu, A perspective for developing polymer-based electromagnetic interference shielding composites, *Nano-Micro Lett.*, 14(2022), No. 1, art. No. 89.

[2] L.G. Ren, Y.Q. Wang, X. Zhang, Q.C. He, and G.L. Wu, Efficient microwave absorption achieved through *in situ* construction of core–shell $CoFe_2O_4$@mesoporous carbon hollow spheres, *Int. J. Miner. Metall. Mater.*, 30(2023), 3, p. 504.

[3] Z.L. Ma, S.L. Kang, J.Z. Ma, *et al*., Ultraflexible and mechanically strong double-layered aramid nanofiber-$Ti_3C_2T_x$ MXene/silver nanowire nanocomposite papers for high-performance electromagnetic interference shielding, *ACS Nano*, 14(2020), No. 7, p. 8368.

[4] Z.L. Ma, X.L. Xiang, L. Shao, Y.L. Zhang, and J.W. Gu, Multifunctional wearable silver nanowire decorated leather nanocomposites for joule heating, electromagnetic interference shielding and piezoresistive sensing, *Angew. Chem. Int. Ed.*, 61(2022), No. 15, art. No. e202200705.

[5] Y. Liu, X.F. Zhou, Z.R. Jia, H.J. Wu, and G.L. Wu, Oxygen vacancy-induced dielectric polarization prevails in the electromagnetic wave-absorbing mechanism for Mn-based MOFs-derived composites, *Adv. Funct. Mater.*, 32(2022), No. 34, art. No. 2204499.

[6] Z.C. Lou, Q.Y. Wang, W. Sun, *et al*., Regulating lignin content to obtain excellent bamboo-derived electromagnetic wave absorber with thermal stability, *Chem. Eng. J.*, 430(2022), art. No. 133178.

[7] X.D. Zhou, H. Han, Y.C. Wang, C. Zhang, H.L. Lv, and Z.C. Lou, Silicon-coated fibrous network of carbon nanotube/iron towards stable and wideband electromagnetic wave absorption, *J. Mater. Sci. Technol.*, 121(2022), p. 199.

[8] Y. Liu, Z. Jia, Q. Zhan, Y. Dong, Q. Xu, and G. Wu, Magnetic manganese-based composites with multiple loss mechanisms towards broadband absorption, *Nano Res.*, 15(2022), No. 6, p. 5590.

[9] S.J. Zhang, Z.R. Jia, B. Cheng, Z.W. Zhao, F. Lu, and G.L. Wu, Recent progress of perovskite oxides and their hybrids for electromagnetic wave absorption: A mini-review, *Adv. Compos. Hybrid Mater.*, 5(2022), No. 3, p. 2440.

[10] Z.C. Lou, Q.Y. Wang, U.I. Kara, *et al*., Biomass-derived carbon heterostructures enable environmentally adaptive wideband electromagnetic wave absorbers, *Nano-Micro Lett.*, 14(2021), No. 1, art. No. 11.

[11] Z.G. Gao, Y.H. Song, S.J. Zhang, *et al*., Electromagnetic absorbers with Schottky contacts derived from interfacial ligand exchanging metal-organic frameworks, *J. Colloid Interface Sci.*, 600(2021), p. 288.

[12] J.K. Liu, Z.R. Jia, W.H. Zhou, *et al*., Self-assembled MoS_2/magnetic ferrite $CuFe_2O_4$ nanocomposite for high-efficiency microwave absorption, *Chem. Eng. J.*, 429(2022), art. No. 132253.

[13] Z.G. Gao, J.Q. Zhang, S.J. Zhang, J. Wang, and Y.H. Song, Cationic etching of ZIF-67 derived $LaCoO_3$/Co_3O_4 as high-efficiency electromagnetic absorbents, *Chem. Eng. J.*, 421(2021), art. No. 127829.

[14] Z.G. Gao, Z.H. Ma, D. Lan, *et al*., Synergistic polarization loss of MoS_2-based multiphase solid solution for electromagnetic wave absorption, *Adv. Funct. Mater.*, 32(2022), No. 18, art. No. 2112294.

[15] Z.H. Zhao, D. Lan, L.M. Zhang, and H.J. Wu, A flexible, mechanically strong, and anti-corrosion electromagnetic wave absorption composite film with periodic electroconductive patterns, *Adv. Funct. Mater.*, 32(2022), No. 15, art. No. 2111045.

[16] S.J. Zhang, B. Cheng, Z.G. Gao, *et al*., Two-dimensional nanomaterials for high-efficiency electromagnetic wave absorption: An overview of recent advances and prospects, *J. Alloys Compd.*, 893(2022), art. No. 162343.

[17] J.L. Liu, Z.H. Zhao, and L.M. Zhang, Toward the application of electromagnetic wave absorption by two-dimension materials, *J. Mater. Sci.: Mater. Electron.*, 32(2021), No. 21, p. 25562.

[18] H. Zhao, J. Yun, Y.L. Zhang, *et al*., Pressure-induced self-interlocked structures for expanded graphite composite papers achieving prominent EMI shielding effectiveness and outstanding thermal conductivities, *ACS Appl. Mater. Interfaces*, 14(2022), No. 2, p. 3233.

[19] S.J. Zhang, Z.G. Gao, Q. Jia, *et al*., Bioinspired strategy for HMX@hBNNS dual shell energetic composites with enhanced desensitization and improved thermal property, *Adv. Mater. Interfaces*, 7(2020), No. 22, art. No. 2001054.

[20] X.Y. Jin, S.W. Wang, C.Y. Sang, *et al*., Patternable nanocellulose/$Ti_3C_2T_x$ flexible films with tunable photoresponsive and electromagnetic interference shielding performances, *ACS Appl. Mater. Interfaces*, 14(2022), No. 30, p. 35040.

[21] S. Manzeli, D. Ovchinnikov, D. Pasquier, O.V. Yazyev, and A. Kis, 2D transition metal dichalcogenides, *Nat. Rev. Mater.*, 2(2017), art. No. 17033.

[22] Q. Fu, J.C. Han, X.J. Wang, *et al*., Electrocatalysts: 2D transition metal dichalcogenides: Design, modulation, and challenges in electrocatalysis, *Adv. Mater.*, 33(2021), No. 6, art. No. 2170045.

[23] Y. Zhou and L.D. Zhao, Promising thermoelectric bulk materials with 2D structures, *Adv. Mater.*, 29(2017), No. 45, art. No. 1702676.

[24] C.Y. Yan, C.H. Gong, P.H. Wang, *et al*., 2D group IVB transition metal dichalcogenides, *Adv. Funct. Mater.*, 28(2018), No. 39, art. No. 1803305.

[25] Z.Z. Zhao, W.H. Liu, Y.W. Jiang, Y.F. Wan, R.H. Du, and H. Li, Solidification of heavy metals in lead smelting slag and development of cementitious materials, *J. Clean. Prod.*, 359(2022), art. No. 132134.

[26] F. Zhang, Z.R. Jia, J.X. Zhou, J.K. Liu, G.L. Wu, and P.F. Yin, Metal-organic framework-derived carbon nanotubes for broadband electromagnetic wave absorption, *Chem. Eng. J.*, 450(2022), art. No. 138205.

[27] D. Voiry, A. Mohite, and M. Chhowalla, Phase engineering of transition metal dichalcogenides, *Chem. Soc. Rev.*, 44(2015), No. 9, p. 2702.

[28] X. Yin, C.S. Tang, Y. Zheng, *et al*., Recent developments in 2D transition metal dichalcogenides: Phase transition and applications of the (quasi-) metallic phases, *Chem. Soc. Rev.*, 50(2021), No. 18, p. 10087.
[29] Z.H. Hu, Z.T. Wu, C. Han, J. He, Z.H. Ni, and W. Chen, Two-dimensional transition metal dichalcogenides: Interface and defect engineering, *Chem. Soc. Rev.*, 47(2018), No. 9, p. 3100.
[30] Z.M. Wei, B. Li, C.X. Xia, *et al*., Various structures of 2D transition-metal dichalcogenides and their applications, *Small Methods*, 2(2018), No. 11, art. No. 1800094.
[31] J. Wang, X.Y. Lin, R.X. Zhang, Z.Y. Chu, and Z.Y. Huang, Transition metal dichalcogenides MX_2 (M = Mo, W; X = S, Se, Te) and MX_2-CIP composites: Promising materials with high microwave absorption performance, *J. Alloys Compd.*, 743(2018), p. 26.
[32] M. Chang, Z.R. Jia, S.Q. He, *et al*., Two-dimensional interface engineering of $NiS/MoS_2/Ti_3C_2T_x$ heterostructures for promoting electromagnetic wave absorption capability, *Composites Part B*, 225(2021), art. No. 109306.
[33] J. Yan, Y. Huang, X.Y. Zhang, *et al*., MoS_2-decorated/integrated carbon fiber: Phase engineering well-regulated microwave absorber, *Nano-Micro Lett.*, 13(2021), No. 1, art. No. 114.
[34] M.H. Li, W.J. Zhu, X. Li, *et al*., $Ti_3C_2T_x/MoS_2$ self-rolling rod-based foam boosts interfacial polarization for electromagnetic wave absorption, *Adv. Sci.*, 9(2022), No. 16, art. No. 2201118.
[35] K. Yang, Y.H. Cui, Z.H. Liu, P. Liu, Q.Y. Zhang, and B.L. Zhang, Design of core–shell structure NC@MoS_2 hierarchical nanotubes as high-performance electromagnetic wave absorber, *Chem. Eng. J.*, 426(2021), art. No. 131308.
[36] M. Qin, L.M. Zhang, and H.J. Wu, Dielectric loss mechanism in electromagnetic wave absorbing materials, *Adv. Sci.*, 9(2022), No. 10, art. No. e2105553.
[37] J. Li, D. Zhou, P.J. Wang, *et al*., Recent progress in two-dimensional materials for microwave absorption applications, *Chem. Eng. J.*, 425(2021), art. No. 131558.
[38] M.S. Cao, J.C. Shu, X.X. Wang, *et al*., Electronic structure and electromagnetic properties for 2D electromagnetic functional materials in gigahertz frequency, *Ann. Phys.*, 531(2019), No. 4, art. No. 1800390.
[39] J. Zhang, J.C. Zhang, X.F. Shuai, *et al*., Design and synthesis strategies: 2D materials for electromagnetic shielding/absorbing, *Chem. Asian J.*, 16(2021), No. 23, p. 3817.
[40] H. Lv, Z. Yang, B. Liu, *et al*., A flexible electromagnetic wave-electricity harvester, *Nat. Commun.*, 12(2021), art. No. 834.
[41] T.Q. Hou, Z.R. Jia, A.L. Feng, *et al*., Hierarchical composite of biomass derived magnetic carbon framework and phytic acid doped polyanilne with prominent electromagnetic wave absorption capacity, *J. Mater. Sci. Technol.*, 68(2021), p. 61.
[42] T.Q. Hou, Z.R. Jia, Y.H. Dong, X.H. Liu, and G.L. Wu, Layered 3D structure derived from MXene/magnetic carbon nanotubes for ultra-broadband electromagnetic wave absorption, *Chem. Eng. J.*, 431(2022), art. No. 133919.
[43] T.Q. Hou, Z.R. Jia, B.B. Wang, *et al*., MXene-based accordion 2D hybrid structure with $Co_9S_8/C/Ti_3C_2T_x$ as efficient electromagnetic wave absorber, *Chem. Eng. J.*, 414(2021), art. No. 128875.
[44] Z.G. Gao, D. Lan, L.M. Zhang, and H.J. Wu, Simultaneous manipulation of interfacial and defects polarization toward Zn/Co phase and ion hybrids for electromagnetic wave absorption, *Adv. Funct. Mater.*, 31(2021), No. 50, art. No. 2106677.
[45] X.L. Chen, Y. Wang, H.L. Liu, S. Jin, and G.L. Wu, Interconnected magnetic carbon@$Ni_xCo_{1-x}Fe_2O_4$ nanospheres with core–shell structure: An efficient and thin electromagnetic wave absorber, *J. Colloid Interface Sci.*, 606(2022), p. 526.
[46] P.F. Yin, G.L. Wu, Y.T. Tang, *et al*., Structure regulation in N-doping biconical carbon frame decorated with $CoFe_2O_4$ and (Fe, Ni) for broadband microwave absorption, *Chem. Eng. J.*, 446(2022), art. No. 136975.
[47] X. Wang, F. Pan, Z. Xiang, *et al*., Magnetic vortex core-shell Fe_3O_4@C nanorings with enhanced microwave absorption performance, *Carbon*, 157(2020), p. 130.
[48] H.L. Lv, X.D. Zhou, G.L. Wu, U.I. Kara, and X.G. Wang, Engineering defects in 2D g-C_3N_4 for wideband, efficient electromagnetic absorption at elevated temperature, *J. Mater. Chem. A*, 9(2021), No. 35, p. 19710.
[49] Y. Zhou, H.P. Wang, D. Wang, *et al*., Insight to the enhanced microwave absorption of porous N-doped carbon driven by ZIF-8: Competition between graphitization and porosity, *Int. J. Miner. Metall. Mater.*, 30(2023), 3, p. 474.
[50] Y.F. Zhang, Y.L. Li, M.M. Wei, D.T. Yang, Q.Y. Zhang, and B.L. Zhang, Core–shell structured Co@NC@MoS_2 magnetic hierarchical nanotubes: Preparation and microwave absorbing properties, *J. Mater. Sci. Technol.*, 128(2022), p. 148.
[51] Y. Liu, X.H. Liu, X.Y. E, *et al*., Synthesis of Mn_xO_y@C hybrid composites for optimal electromagnetic wave absorption capacity and wideband absorption, *J. Mater. Sci. Technol.*, 103(2022), p. 157.
[52] Z.R. Jia, M.Y. Kong, B.W. Yu, Y.Z. Ma, J.Y. Pan, and G.L. Wu, Tunable Co/ZnO/C@MWCNTs based on carbon nanotube-coated MOF with excellent microwave absorption properties, *J. Mater. Sci. Technol.*, 127(2022), p. 153.
[53] Y.M. Luo, P.F. Yin, G.L. Wu, *et al*., Porous carbon sphere decorated with Co/Ni nanoparticles for strong and broadband electromagnetic dissipation, *Carbon*, 197(2022), p. 389.
[54] Z.C. Lou, Q.Y. Wang, X.D. Zhou, *et al*., An angle-insensitive electromagnetic absorber enabling a wideband absorption, *J. Mater. Sci. Technol.*, 113(2022), p. 33.
[55] L.L. Xu, J.Q. Tao, X.F. Zhang, *et al*., Hollow C@MoS_2 nanospheres for microwave absorption, *ACS Appl. Nano Mater.*, 4(2021), No. 10, p. 11199.
[56] X.R. Gao, Z.R. Jia, B.B. Wang, *et al*., Synthesis of NiCo-LDH/MXene hybrids with abundant heterojunction surfaces as a lightweight electromagnetic wave absorber, *Chem. Eng. J.*, 419(2021), art. No. 130019.
[57] S.J. Zhang, Y.X. Pei, Z.Z. Zhao, C.L. Guan, and G.L. Wu, Simultaneous manipulation of polarization relaxation and conductivity toward self-repairing reduced graphene oxide based ternary hybrids for efficient electromagnetic wave absorption, *J. Colloid Interface Sci.*, 630(2023), p. 453.
[58] X.L. Cao, Z.R. Jia, D.Q. Hu, and G.L. Wu, Synergistic construction of three-dimensional conductive network and double heterointerface polarization via magnetic FeNi for broadband microwave absorption, *Adv. Compos. Hybrid Mater.*, 5(2022), No. 2, p. 1030.
[59] X.Y. Zhang, Z.R. Jia, F. Zhang, *et al*., MOF-derived $NiFe_2S_4$/Porous carbon composites as electromagnetic wave absorber, *J. Colloid Interface Sci.*, 610(2022), p. 610.
[60] J. Wang, Z. Jia, X. Liu, *et al*., Construction of 1D heterostructure NiCo@C/ZnO nanorod with enhanced microwave absorption, *Nano-Micro Lett*, 13(2021), No. 1, art. No. 175.
[61] Y. He, Y. Wang, L. Ren, *et al*., Construction of heterointerfaces and honeycomb-like structure for ultrabroad microwave absorption, *J. Colloid Interface Sci.*, 627(2022), p. 102.
[62] Y.Q. Guo, H. Qiu, K.P. Ruan, S.S. Wang, Y.L. Zhang, and J.W. Gu, Flexible and insulating silicone rubber composites with sandwich structure for thermal management and electromagnetic interference shielding, *Compos. Sci. Technol.*, 219(2022), art. No. 109253.
[63] T.T. Zheng, Z.R. Jia, Q.Q. Zhan, *et al*., Self-assembled multilayered hexagonal-like MWCNTs/MnF_2/CoO nanocomposite with enhanced electromagnetic wave absorption, *Carbon*,

186(2022), p. 262.
[64] F. Zhang, Z.R. Jia, Z. Wang, *et al*., Tailoring nanoparticles composites derived from metal-organic framework as electromagnetic wave absorber, *Mater. Today Phys.*, 20(2021), art. No. 100475.
[65] C.X. Wang, Z.R. Jia, S.Q. He, *et al*., Metal-organic framework-derived CoSn/NC nanocubes as absorbers for electromagnetic wave attenuation, *J. Mater. Sci. Technol.*, 108(2022), p. 236.
[66] L.F. Sun, Z.R. Jia, S. Xu, *et al*., Synthesis of $NiCo_{2-0.5x}Cr_2O_3$@C nanoparticles based on hydroxide with the heterogeneous interface for excellent electromagnetic wave absorption properties, *Compos. Commun.*, 29(2022), art. No. 100993.
[67] Y.T. Zhou, Z.Y. Bai, X.Y. Yang, *et al*., *In-situ* grown of NiCo bimetal anchored on porous straw-derived biochar composites with boosted microwave absorption properties, *Int. J. Miner. Metall. Mater.*, 30(2023), 3, p. 515.
[68] Y. Liu, J.G. Qin, L.L. Lu, J. Xu, and X.L. Su, Enhanced microwave absorption property of silver decorated biomass ordered porous carbon composite materials with frequency selective surface incorporation, *Int. J. Miner. Metall. Mater.*, 30(2023), 3, p. 525.
[69] Z.H. Zhao, X.J. Zhou, K.C. Kou, and H.J. Wu, PVP-assisted transformation of ZIF-67 into cobalt layered double hydroxide/carbon fiber as electromagnetic wave absorber, *Carbon*, 173(2021), p. 80.
[70] Z.H. Zhao, K.C. Kou, L.M. Zhang, and H.J. Wu, Optimal particle distribution induced interfacial polarization in bouquet-like hierarchical composites for electromagnetic wave absorption, *Carbon*, 186(2022), p. 323.
[71] H.X. Zhang, Z.R. Jia, B.B. Wang, *et al*., Construction of remarkable electromagnetic wave absorber from heterogeneous structure of Co-$CoFe_2O_4$@mesoporous hollow carbon spheres, *Chem. Eng. J.*, 421(2021), art. No. 129960.
[72] H.X. Zhang, Z.R. Jia, A.L. Feng, *et al., In situ* deposition of pitaya-like Fe_3O_4@C magnetic microspheres on reduced graphene oxide nanosheets for electromagnetic wave absorber, *Composites Part B*, 199(2020), art. No. 108261.
[73] X. Feng, P.F. Yin, L.M. Zhang, *et al*., Innovative preparation of Co@$CuFe_2O_4$ composite via ball-milling assisted chemical precipitation and annealing for glorious electromagnetic-wave absorption, *Int. J. Miner. Metall. Mater.*, 30(2023), 3, p. 559.
[74] L. Chai, Y.Q. Wang, Z.R. Jia, *et al*., Tunable defects and interfaces of hierarchical dandelion-like $NiCo_2O_4$ *via* Ostwald ripening process for high-efficiency electromagnetic wave absorption, *Chem. Eng. J.*, 429(2022), art. No. 132547.
[75] Z.X. Liu, Y.Q. Wang, Z.R. Jia, *et al., In situ* constructed honeycomb-like $NiFe_2O_4$@Ni@C composites as efficient electromagnetic wave absorber, *J. Colloid Interface Sci.*, 608(2022), p. 2849.
[76] C.H. Sun, Z.R. Jia, S. Xu, D.Q. Hu, C.H. Zhang, and G.L. Wu, Synergistic regulation of dielectric-magnetic dual-loss and triple heterointerface polarization via magnetic MXene for high-performance electromagnetic wave absorption, *J. Mater. Sci. Technol.*, 113(2022), p. 128.
[77] L. Chai, Y.Q. Wang, N.F. Zhou, *et al., In-situ* growth of core-shell $ZnFe_2O_4$@ porous hollow carbon microspheres as an efficient microwave absorber, *J. Colloid Interface Sci.*, 581(2021), p. 475.
[78] L. Kong, S.H. Luo, S.Y. Zhang, G.Q. Zhang, Y. Zhang, Ultralight pyrolytic carbon foam reinforced with amorphous carbon nanotubes for broadband electromagnetic absorption, *Int. J. Miner. Metall. Mater.*, 30(2023), 3, p. 570.
[79] L.G. Ren, Y.Q. Wang, Z.R. Jia, Q.C. He, and G.L. Wu, Controlling the heterogeneous interfaces of Fe_3O_4/N-doped porous carbon *via* facile swelling for enhancing the electromagnetic wave absorption, *Compos. Commun.*, 29(2022), art. No. 101052.
[80] X.M. Huang, X.H. Liu, Z.R. Jia, B.B. Wang, X.M. Wu, and G.L. Wu, Synthesis of 3D cerium oxide/porous carbon for enhanced electromagnetic wave absorption performance, *Adv. Compos. Hybrid Mater.*, 4(2021), No. 4, p. 1398.
[81] Z.G. Gao, Z.H. Zhao, D. Lan, K.C. Kou, J.Q. Zhang, and H.J. Wu, Accessory ligand strategies for hexacyanometallate networks deriving perovskite polycrystalline electromagnetic absorbents, *J. Mater. Sci. Technol.*, 82(2021), p. 69.
[82] H.R. Geng, X. Zhang, W.H. Xie, *et al*., Lightweight and broadband 2D MoS_2 nanosheets/3D carbon nanofibers hybrid aerogel for high-efficiency microwave absorption, *J. Colloid Interface Sci.*, 609(2022), p. 33.
[83] X. Sun, Y.H. Pu, F. Wu, *et al*., 0D–1D–2D multidimensionally assembled Co_9S_8/CNTs/MoS_2 composites for ultralight and broadband electromagnetic wave absorption, *Chem. Eng. J.*, 423(2021), art. No. 130132.
[84] W. Ding, L. Hu, Q.C. Liu, *et al*., Structure modulation induced enhancement of microwave absorption in WS_2 nanosheets, *Appl. Phys. Lett.*, 113(2018), No. 24, art. No. 243102.
[85] M.Q. Ning, P.H. Jiang, W. Ding, *et al*., Phase manipulating toward molybdenum disulfide for optimizing electromagnetic wave absorbing in gigahertz, *Adv. Funct. Mater.*, 31(2021), No. 19, art. No. 2011229.
[86] H.B. Zhang, J.Y. Cheng, H.H. Wang, *et al*., Initiating VB-group laminated NbS_2 electromagnetic wave absorber toward superior absorption bandwidth as large as 6.48 GHz through phase engineering modulation, *Adv. Funct. Mater.*, 32(2022), No. 6, art. No. 2108194.
[87] Y.C. Cheng, Z.Y. Zhu, W.B. Mi, Z.B. Guo, and U. Schwingenschlögl, Prediction of two-dimensional diluted magnetic semiconductors: Doped monolayer MoS_2 systems, *Phys. Rev. B*, 87(2013), No. 10, art. No. 100401.
[88] J. Wang, X.Y. Lin, Z.Y. Chu, *et al*., Magnetic MoS_2: A promising microwave absorption material with both dielectric loss and magnetic loss properties, *Nanotechnology*, 31(2020), No. 13, art. No. 135602.
[89] L.L. Liang, W.H. Gu, Y. Wu, *et al*., Heterointerface engineering in electromagnetic absorbers: New insights and opportunities, *Adv. Mater.*, 34(2022), No. 4, art. No. e2106195.
[90] Z. Feng, P.P. Yang, G.S. Wen, H.B. Li, Y. Liu, and X.C. Zhao, One-step synthesis of MoS_2 nanoparticles with different morphologies for electromagnetic wave absorption, *Appl. Surf. Sci.*, 502(2020), art. No. 144129.
[91] Y. Xia, W.F. Zhu, Q. Zhu, *et al*., Investigation on the critical factors of $MoSe_2$-based microwave absorbing property, *J. Mater. Sci.: Mater. Electron.*, 32(2021), No. 21, p. 25795.
[92] Y. Cheng, Y. Zhao, H.Q. Zhao, *et al*., Engineering morphology configurations of hierarchical flower-like $MoSe_2$ spheres enable excellent low-frequency and selective microwave response properties, *Chem. Eng. J.*, 372(2019), p. 390.
[93] M. Wu, Y. Zheng, X.H. Liang, *et al*., MoS_2 nanostructures with the 1T phase for electromagnetic wave absorption, *ACS Appl. Nano Mater.*, 4(2021), No. 10, p. 11042.
[94] L.S. Xing, X. Li, Z.C. Wu, *et al*., 3D hierarchical local heterojunction of MoS_2/FeS_2 for enhanced microwave absorption, *Chem. Eng. J.*, 379(2020), art. No. 122241.
[95] J.J. Zhang, X.S. Qi, X. Gong, *et al*., Microstructure optimization of core@shell structured MSe_2/$FeSe_2$@$MoSe_2$ (M = Co, Ni) flower-like multicomponent nanocomposites towards high-efficiency microwave absorption, *J. Mater. Sci. Technol.*, 128(2022), p. 59.
[96] J.J. Zhang, Z.H. Li, X.S. Qi, *et al*., Constructing flower-like core@shell $MoSe_2$-based nanocomposites as a novel and high-efficient microwave absorber, *Composites Part B*, 222(2021),

art. No. 109067.
[97] A.K. Darboe, X.S. Qi, X. Gong, *et al*., Constructing $MoSe_2/MoS_2$ and $MoS_2/MoSe_2$ inner and outer-interchangeable flower-like heterojunctions: A combined strategy of interface polarization and morphology configuration to optimize microwave absorption performance, *J. Colloid Interface Sci.*, 624(2022), p. 204.
[98] S.J. Zhang, B. Cheng, Z.R. Jia, *et al*., The art of framework construction: Hollow-structured materials toward high-efficiency electromagnetic wave absorption, *Adv. Compos. Hybrid Mater.*, 5(2022), No. 3, p. 1658.
[99] D.Q. Zhang, Y.F. Xiong, J.Y. Cheng, *et al*., Construction of low-frequency and high-efficiency electromagnetic wave absorber enabled by texturing rod-like TiO_2 on few-layer of WS_2 nanosheets, *Appl. Surf. Sci.*, 548(2021), art. No. 149158.
[100] H. Chen, J. Shen, and Y.H. Zhang, Preparation and microwave absorption characteristics of $MoS_2/Nd_2O_2CO_3$ composites, *J. Mater. Sci.: Mater. Electron.*, 33(2022), No. 8, p. 4902.
[101] J.H. Luo, K. Zhang, M.L. Cheng, M.M. Gu, and X.K. Sun, MoS_2 spheres decorated on hollow porous ZnO microspheres with strong wideband microwave absorption, *Chem. Eng. J.*, 380(2020), art. No. 122625.
[102] P. Song, B. Liu, C.B. Liang, *et al*., Lightweight, flexible cellulose-derived carbon aerogel@reduced graphene oxide/PDMS composites with outstanding EMI shielding performances and excellent thermal conductivities, *Nano-Micro Lett.*, 13(2021), No. 1, art. No. 91.
[103] Y.H. Song, X.H. Liu, Z.G. Gao, *et al*., Core–shell Ag@C spheres derived from Ag-MOFs with tunable ligand exchanging phase inversion for electromagnetic wave absorption, *J. Colloid Interface Sci.*, 620(2022), p. 263.
[104] J.H. Luo, M.N. Feng, Z.Y. Dai, C.Y. Jiang, W. Yao, and N.X. Zhai, MoS_2 wrapped MOF-derived N-doped carbon nanocomposite with wideband electromagnetic wave absorption, *Nano Res.*, 15(2022), No. 7, p. 5781.
[105] C.X. Hou, J.Y. Cheng, H.B. Zhang, *et al*., Biomass-derived carbon-coated WS_2 core-shell nanostructures with excellent electromagnetic absorption in C-band, *Appl. Surf. Sci.*, 577(2022), art. No. 151939.
[106] W.D. Zhang, X. Zhang, Q. Zhu, Y. Zheng, L.F. Liotta, and H.J. Wu, High-efficiency and wide-bandwidth microwave absorbers based on MoS_2-coated carbon fiber, *J. Colloid Interface Sci.*, 586(2021), p. 457.
[107] L.F. Lyu, F.L. Wang, B. Li, *et al*., Constructing 1T/2H MoS_2 nanosheets/3D carbon foam for high-performance electromagnetic wave absorption, *J. Colloid Interface Sci.*, 586(2021), p. 613.
[108] F. Pan, Z. Liu, B. Deng, *et al*., Lotus leaf-derived gradient hierarchical porous C/MoS_2 morphology genetic composites with wideband and tunable electromagnetic absorption performance, *Nano-Micro Lett*, 13(2021), No. 1, art. No. 43.
[109] Z.J. Xu, M. He, Y.M. Zhou, *et al*., Spider web-like carbonized bacterial cellulose/$MoSe_2$ nanocomposite with enhanced microwave attenuation performance and tunable absorption bands, *Nano Res.*, 14(2021), No. 3, p. 738.
[110] D.Q. Zhang, T.T. Liu, J.Y. Cheng, *et al*., Lightweight and high-performance microwave absorber based on 2D WS_2-RGO heterostructures, *Nano-Micro Lett.*, 11(2019), No. 1, art. No. 38.
[111] D.Q. Zhang, H.H. Wang, J.Y. Cheng, *et al*., Conductive WS_2-NS/CNTs hybrids based 3D ultra-thin mesh electromagnetic wave absorbers with excellent absorption performance, *Appl. Surf. Sci.*, 528(2020), art. No. 147052.
[112] Y.H. Han, J. Yuan, Y.H. Zhu, Q.Q. Wang, L. Li, and M.S. Cao, Implantation of WSe_2 nanosheets into multi-walled carbon nanotubes for enhanced microwave absorption, *J. Colloid Interface Sci.*, 609(2022), p. 746.
[113] Y.H. Zhu, Q.Q. Wang, Y.H. Han, L. Li, and M.S. Cao, Constructing WSe_2@CNTs heterojunction to tune attenuation capability for efficient microwave absorbing and green EMI shielding, *Appl. Surf. Sci.*, 592(2022), art. No. 153253.
[114] R. Wang, E.Q. Yang, X.S. Qi, *et al*., Constructing and optimizing core@shell structure CNTs@MoS_2 nanocomposites as outstanding microwave absorbers, *Appl. Surf. Sci.*, 516(2020), art. No. 146159.
[115] J. Xu, L.N. Liu, X.C. Zhang, *et al*., Tailoring electronic properties and polarization relaxation behavior of MoS_2 monolayers for electromagnetic energy dissipation and wireless pressure micro-sensor, *Chem. Eng. J.*, 425(2021), art. No. 131700.
[116] W.L. Zhang, D.G. Jiang, X.X. Wang, B.N. Hao, Y. Liu, and J.Q. Liu, Growth of polyaniline nanoneedles on MoS_2 nanosheets, tunable electroresponse, and electromagnetic wave attenuation analysis, *J. Phys. Chem. C*, 121(2017), p. 4989.
[117] X.L. Wang, C.J. Li, H.R. Geng, *et al*., Tunable dielectric properties and electromagnetic wave absorbing performance of MoS_2/Fe_3O_4/PANI composite, *Colloids Surface A*, 637(2022), art. No. 128285.
[118] J.L. Ma, H.D. Ren, Z.Y. Liu, *et al*., Embedded MoS_2–PANI nanocomposites with advanced microwave absorption performance, *Compos. Sci. Technol.*, 198(2020), art. No. 108239.
[119] Q. Su, B.C. Wang, C.P. Mu, *et al*., Polypyrrole coated 3D flower MoS_2 composites with tunable impedance for excellent microwave absorption performance, *J. Alloys Compd.*, 888(2021), art. No. 161487.
[120] L.X. Gai, Y.M. Zhao, G.L. Song, *et al*., Construction of core-shell PPy@MoS_2 with nanotube-like heterostructures for electromagnetic wave absorption: Assembly and enhanced mechanism, *Composites Part A*, 136(2020), art. No. 105965.
[121] Y.L. Zhang, Y. Yan, H. Qiu, Z.L. Ma, K.P. Ruan, and J.W. Gu, A mini-review of MXene porous films: Preparation, mechanism and application, *J. Mater. Sci. Technol.*, 103(2022), p. 42.
[122] P. Song, B. Liu, H. Qiu, X.T. Shi, D.P. Cao, and J.W. Gu, MXenes for polymer matrix electromagnetic interference shielding composites: A review, *Compos. Commun.*, 24(2021), art. No. 100653.
[123] Q.Q. Chen, S. Bao, F.C. Wei, *et al*., Promoting the electromagnetic interference shielding of $Ti_3C_2T_x$ flakes by loading Fe_3O_4 nanoparticles: Insights into the performance of oligolayers exposed to microwave interferences, *Ceram. Int.*, 48(2022), No. 17, p. 24656.
[124] P. He, M.J. Zheng, Q. Liu, *et al*., MXene nanohybrids: Excellent electromagnetic properties for absorbing electromagnetic waves, *Ceram. Int.*, 48(2022), No. 2, p. 1484.
[125] A. Hassan, M.A. Aslam, M. Bilal, *et al*., Modulating dielectric loss of MoS_2@$Ti_3C_2T_x$ nanoarchitectures for electromagnetic wave absorption with radar cross section reduction performance verified through simulations, *Ceram. Int.*, 47(2021), No. 14, p. 20706.
[126] Z.H. Liu, Y.H. Cui, Q. Li, Q.Y. Zhang, and B.L. Zhang, Fabrication of folded MXene/MoS_2 composite microspheres with optimal composition and their microwave absorbing properties, *J. Colloid Interface Sci.*, 607(2022), p. 633.
[127] X. Li, C.Y. Wen, L.T. Yang, R.X. Zhang, Y.S. Li, and R.C. Che, Enhanced visualizing charge distribution of 2D/2D MXene/MoS_2 heterostructure for excellent microwave absorption performance, *J. Alloys Compd.*, 869(2021), art. No. 159365.
[128] H.D. Ren, S. Wang, X.M. Zhang, *et al*., Broadband electromagnetic absorption of $Ti_3C_2T_x$ MXene/WS_2 composite *via* constructing two-dimensional heterostructure, *J. Am. Ceram. Soc.*, 104(2021), No. 11, p. 5537.

[129] J. Yang, J. Wang, H. Li, *et al*., MoS_2/MXene aerogel with conformal heterogeneous interfaces tailored by atomic layer deposition for tunable microwave absorption, *Adv. Sci.*, 9(2022), No. 7, art. No. e2101988.

[130] J.X. Chai, J.Y. Cheng, D.Q. Zhang, *et al*., Enhancing electromagnetic wave absorption performance of Co_3O_4 nanoparticles functionalized MoS_2 nanosheets, *J. Alloys Compd.*, 829(2020), art. No. 154531.

[131] D.Q. Zhang, Y.F. Xiong, J.Y. Cheng, *et al*., Synergetic dielectric loss and magnetic loss towards superior microwave absorption through hybridization of few-layer WS_2 nanosheets with NiO nanoparticles, *Sci. Bull.*, 65(2020), No. 2, p. 138.

[132] H.M. Liu, M. Zhang, Y.F. Ye, J.L. Yi, Y.X. Zhang, and Q.C. Liu, Porous cobalt ferrite microspheres decorated two-dimensional MoS_2 as an efficient and wideband microwave absorber, *J. Alloys Compd.*, 892(2022), art. No. 162126.

[133] M. Wu, X.H. Liang, Y. Zheng, C.Y. Qian, and D.H. Wang, Excellent microwave absorption performances achieved by optimizing core@shell structures of Fe_3O_4@1T/2H-MoS_2 composites, *J. Alloys Compd.*, 910(2022), art. No. 164881.

[134] M. Ma, Q. Zheng, Y.H. Zhu, L. Li, and M.S. Cao, Confinedly implanting Fe_3O_4 nanoclusters on MoS_2 nanosheets to tailor electromagnetic properties for excellent multi-bands microwave absorption, *J. Materiomics*, 8(2022), No. 3, p. 577.

[135] F. Hu, J.X. Dai, Q. Liu, Z.Q. Zhang, and G.L. Xu, Synthesis of flowerlike MoS_2/CoNi composites for enhancing electromagnetic wave absorption, *Acta Metall. Sin.*, 35(2022), No. 6, p. 890.

[136] M.Q. Wang, Y. Lin, H.B. Yang, Y. Qiu, and S. Wang, A novel plate-like $BaFe_{12}O_{19}$@MoS_2 core–shell structure composite with excellent microwave absorbing properties, *J. Alloys Compd.*, 817(2020), art. No. 153265.

[137] Y. Wang, X.C. Di, Y.Q. Fu, X.M. Wu, and J.T. Cao, Facile synthesis of the three-dimensional flower-like $ZnFe_2O_4$@MoS_2 composite with heterogeneous interfaces as a high-efficiency absorber, *J. Colloid Interface Sci.*, 587(2021), p. 561.

[138] X.Y. Wang, T. Zhu, S.C. Chang, Y.K. Lu, W.B. Mi, and W. Wang, 3D Nest-like architecture of core–shell $CoFe_2O_4$@1T/2H-MoS_2 composites with tunable microwave absorption performance, *ACS Appl. Mater. Interfaces*, 12(2020), No. 9, p. 11252.

[139] C.L. Li, M.X. Piao, H. Zhang, and X. Wang, Constructing of Co nanosheets decorating with WS_2 nanoclusters for enhanced electromagnetic wave absorption, *J. Alloys Compd.*, 912(2022), art. No. 165269.

[140] Y.X. Bi, M.L. Ma, Y.Y. Liu, *et al*., Microwave absorption enhancement of 2-dimensional CoZn/C@MoS_2@PPy composites derived from metal-organic framework, *J. Colloid Interface Sci.*, 600(2021), p. 209.

[141] Z.J. Liao, M.L. Ma, Y.X. Bi, *et al*., MoS_2 decorated on one-dimensional $MgFe_2O_4$/MgO/C composites for high-performance microwave absorption, *J. Colloid Interface Sci.*, 606(2022), p. 709.

[142] Z.J. Liao, M.L. Ma, Z.Y. Tong, *et al*., Fabrication of one-dimensional $ZnFe_2O_4$@carbon@MoS_2/FeS_2 composites as electromagnetic wave absorber, *J. Colloid Interface Sci.*, 600(2021), p. 90.

[143] W.B. Huang, Z.Y. Tong, Y.X. Bi, *et al*., Synthesis and microwave absorption properties of coralloid core–shell structure NiS/Ni_3S_4@PPy@MoS_2 nanowires, *J. Colloid Interface Sci.*, 599(2021), p. 262.

[144] Z.H. Qin, C.Y. Wang, Y.Y. Ma, *et al*., MoS_2 nanoflowers decorated with Fe_3O_4/graphite nanosheets for controllable electromagnetic wave absorption, *ACS Appl. Nano Mater.*, 4(2021), No. 4, p. 3434.

[145] X.L. Chen, T. Shi, G.L. Wu, and Y. Lu, Design of molybdenum disulfide@polypyrrole compsite decorated with Fe_3O_4 and superior electromagnetic wave absorption performance, *J. Colloid Interface Sci.*, 572(2020), p. 227.

[146] X.L. Chen, W. Wang, T. Shi, G.L. Wu, and Y. Lu, One pot green synthesis and EM wave absorption performance of MoS_2@nitrogen doped carbon hybrid decorated with ultrasmall cobalt ferrite nanoparticles, *Carbon*, 163(2020), p. 202.

[147] J. Li, D. Zhou, M.S. Fu, *et al*., Coral-like polypyrrole/$LiFe_5O_8$/MoS_2 nanocomposites for high-efficiency microwave absorbers, *ACS Appl. Nano Mater.*, 5(2022), No. 6, p. 7944.

[148] C.Y. Wang, Y.Y. Ma, Z.H. Qin, J.J. Wang, and B. Zhong, Synthesis of hollow spherical MoS_2@Fe_3O_4–GNs ternary composites with enhanced microwave absorption performance, *Appl. Surf. Sci.*, 569(2021), art. No. 150812.

[149] M.Q. Ning, Z.K. Lei, G.G. Tan, Q.K. Man, J.B. Li, and R.W. Li, Dumbbell-like Fe_3O_4@N-doped carbon@2H/1T-MoS_2 with tailored magnetic and dielectric loss for efficient microwave absorbing, *ACS Appl. Mater. Interfaces*, 13(2021), No. 39, p. 47061.

[150] H. Du, Q.P. Zhang, B. Zhao, *et al*., Novel hierarchical structure of MoS_2/TiO_2/$Ti_3C_2T_x$ composites for dramatically enhanced electromagnetic absorbing properties, *J. Adv. Ceram.*, 10(2021), No. 5, p. 1042.

[151] R.R. Yu, Y.H. Xia, X.Y. Pei, *et al*., Micro-flower like core–shell structured ZnCo@C@1T-2H-MoS_2 composites for broadband electromagnetic wave absorption and photothermal performance, *J. Colloid Interface Sci.*, 622(2022), p. 261.

[152] Z.Q. Yang, H.Q. Guo, W.B. You, *et al*., Compressible and flexible PPy@MoS_2/C microwave absorption foam with strong dielectric polarization from 2D semiconductor intermediate sandwich structure, *Nanoscale*, 13(2021), No. 9, p. 5115.